ASTRONOMY & ASTROPHYSICS
SUPPLEMENT SERIES

Astron. Astrophys. Suppl. Ser. **142**, 181–215 (2000)

A $\lambda 2$ mm molecular line survey of the C-star envelope IRC+10216⋆

J. Cernicharo[1], **M. Guélin**[2], **and C. Kahane**[3]

[1] CSIC, Instituto de Estructura de la Materia, C/Serrano 121, 28006 Madrid, Spain
e-mail: cerni@astro.iem.csic.es
[2] IRAM, Domaine Universitaire de Grenoble, 300 rue de la Piscine, 38406 St Martin d'Hères, France
e-mail: guelin@iram.fr
[3] Laboratoire d'Astrophysique de l'Observatoire de Grenoble, BP. 53, 38041 Grenoble Cedex, France

Received April 23; accepted August 6, 1999

Abstract. The mm-wave spectrum of the C-star envelope IRC+10216 has been continuously surveyed between 129.0 and 172.5 GHz with the IRAM 30-m telescope. 380 lines are detected, of which 317 have been identified. The identified lines arise from 30 different molecules and radicals which, in their vast majority, are not observed in hot and dense interstellar clouds such as Orion A or W3(OH). Actually, half of the molecular species identified in the mm-wave spectrum of IRC+10216 were first observed in the course of this spectral survey.

The new species include several carbon-chain molecules and radicals, as well as silicon and metallic compounds. They also include molecules containing rare isotopes of C, Mg, Si, S and Cl, whose elemental abundance ratios in the envelope are redetermined. We observe, in particular, four ^{13}C isotopomers of C_4H, three of C_3N and HC_3N, and four doubly-substituted isotopomers of SiS and CS.

63 lines remain unidentified. Probably, a large fraction of those are rotational transitions inside the excited bending states of the abundant species NaCN, C_5H, and C_6H. We can also expect some lines to be ground state transitions of poorly known silicon and metal compounds, such as the slightly asymmetrical top molecule SiCSi.

Key words: line identification — surveys — stars: AGB and post-AGB — stars: carbon — stars: circumstellar matter — stars: individual: IRC+10216 — ISM: molecules — radio lines: stars

Send offprint requests to: J. Cernicharo

⋆ Tables 2 to 9 are only available in electronic form at the CDS via anonymous ftp to cdsarc.u-strasbg.fr (130.79.128.5) or via http://cdsweb.u-strasbg.fr/Abstract.html or http://www.edpsciences.org

1. Introduction

The nearby carbon-star CW Leo/IRC+10216 has experienced a phase of high mass loss for the last $\sim 10^5$ years and is at the verge of evolving toward a Planetary Nebula. As attested by its non-solar isotopic composition, it has already expelled most of its convective shell in the form of a thick, slowly expanding circumstellar envelope (CSE), formed of molecules and dust grains. This CSE is one of the brightest 10 μm objects and one of the richest molecular sources in the sky: to date, over 53 molecular species have been detected in this object (Table 1).

In view of the wide range of physical conditions present in the stellar atmosphere and in the envelope, the molecules form through a variety of chemical processes: 3-body processes in the hot and dense atmosphere of the star ($R = R_*$), surface reactions in the dust condensation region ($R = 3 - 10\ R_*$), gas phase neutral–neutral or ion–molecule reactions in the CSE ($R \geq 100\ R_*$; see e.g. Glassgold 1996). The molecules present in the atmosphere and in the dust condensation region are best detected through their ro-vibrational lines in the infrared; those present in the cold CSE are best observed through their rotational lines at millimeter wavelengths. Because the molecular rotational temperatures in the CSE are between 10 and 50 K, most molecules, including the small carbon chains and the small metal compounds, have their strongest lines around 2 mm.

Several spectral line surveys of IRC+10216 have been reported in the literature. They include the far Infrared survey with the Infrared Space Obseravtory (ISO) (Cernicharo et al. 1996), the 0.8 mm James Clerk Maxwell Telescope (JCMT) and Caltech Submillimeter Observatory (CSO) surveys (Avery et al. 1992; Groesbeck et al. 1994), the $3-4$ mm Onsala survey (Johansson et al. 1985) and the $6-10$ mm Nobeyama survey (Kawaguchi et al. 1995). In this article, we present the results of a systematic spectral survey of the $2.3-1.7$ mm window.

Table 1. Molecules in this 2 mm line survey of IRC+10216

Molecule	Isotopomer or v-state	Number of Observed Transitions	Table	Previous IRAM data[1]
SiS	SiS	2	4	this work
	^{29}SiS	2	4	Kahane et al. 1988, 1992
	^{30}SiS	2	4	Kahane et al. 1988, 1992
	Si^{34}S	2	4	Kahane et al. 1988, 1992
	Si^{33}S	2	4	Kahane et al. 1988, 1992
	^{29}Si^{34}S	2	4	this work
	^{30}Si^{34}S	1	4	this work
	SiS $v = 1$	2	4	this work
	SiS $v = 2$	2	4	this work
	SiS $v = 3$	1	4	this work
SiO	SiO	1	4	this work
	^{29}SiO	1	4	Kahane et al. 1988, 1992
	^{30}SiO	1	4	Kahane et al. 1988, 1992
SiC	SiC	3	4	Cernicharo et al. 1989, 1992
SiN	SiN	5	4	this work
SiC_2	SiC_2	12	5	this work
	SiC_2 $\nu_3 = 1$	2	5	this work
	$^{29}SiC_2$	11	5	Cernicharo et al. 1986c
	$^{30}SiC_2$	8	5	Cernicharo et al. 1986c
	Si^{13}CC	16	5	Cernicharo et al. 1991a
SiC_3	SiC_3	5	5	this work
ClNa	ClNa	4	6	Cernicharo & Guélin 1987
	^{37}ClNa	2	6	Cernicharo & Guélin 1987
ClK	ClK	4	6	Cernicharo & Guélin 1987
	^{37}ClK	2	6	this work
ClAl	ClAl	2	6	Cernicharo & Guélin 1987
	^{37}ClAl	3	6	this work
AlF	AlF	2	6	Cernicharo & Guélin 1987
MgNC	MgNC	6	6	Guélin et al. 1986
	^{26}MgNC	2	6	Guélin et al. 1995
	^{25}MgNC	1	6	Guélin et al. 1995
NaCN	NaCN	26	6	this work
C_3H	C_3H	8	7	this work
	C_3H $\nu_4 = 1$	4	7	this work
c-C_3H	c-C_3H	8	7	this work
C_3H_2	C_3H_2	4	7	this work
	C^{13}CH_2	1	7	this work
H_2C_4	H_2C_4	12	7	Cernicharo et al. 1991b
C_4H	C_4H	10	7	this work
	C_4H $\nu_7 = 1$	20	7	Guélin et al. 1987
	C_4H $\nu_7 = 2$	17	7	Guélin et al. 1987
	^{13}CCCCH	1	7	this work
	C^{13}CCCH	3	7	this work
	CC^{13}CCH	2	7	this work
	CCC^{13}CH	6	7	this work
C_5H	C_5H	4	7	Cernicharo et al. 1986a,b, 1987a
C_6H	C_6H	18	7	Guélin et al. 1987a & Cernicharo et al. 1987b
HCCN	HCCN	4	8	Guélin & Cernicharo 1991
CH_3CN	CH_3CN	5	8	this work
HC_3N	HC_3N	4	8	this work
	HC_3N $\nu_7 = 1$	5	8	this work
	H^{13}CCCN	4	8	this work
	HC^{13}CCN	4	8	this work
	HCC^{13}CN	4	8	this work
HC_5N	HC_5N	5	8	this work
C_3N	C_3N	8	8	this work
	^{13}CCCN	4	8	this work
	C^{13}CCN	4	8	this work
	CC^{13}CN	2	8	this work

Table 1. continued

Molecule	Isotopomer or v-state	Number of Observed Transitions	Table	Previous IRAM data[1]
CP	CP	4	9	Guélin et al. 1990
PN	PN	1	9	this work
CS	CS	1	9	this work
	CS $v = 1$	1	9	this work
	^{13}CS	1	9	Kahane et al. 1988
	C^{34}S	1	9	Kahane et al. 1988
	C^{33}S	1	9	Kahane et al. 1988
	^{13}C^{34}S	1	9	Kahane et al. 1988
C_2S	C_2S	8	9	Cernicharo et al. 1987c
C_3S	C_3S	5	9	Cernicharo et al. 1987c
	$C_3^{34}S$	1	9	this work
H_2S	H_2S	1	9	this work

(1) Reference to previous publications of partial data from this line survey.

Other species in IRC+10216 not in this 2 mm survey:

NH_3	SiH_4					
CN	CO	HCN	HNC	HCO^+	CH_4	MgCN
C_2	C_2H	HCCH	H_2CCH_2			
C_3	H_2C_3					
C_4Si						
C_5	C_5N					
H_2C_6						
C_7H	HC_7N					
C_8H						
HC_9N						

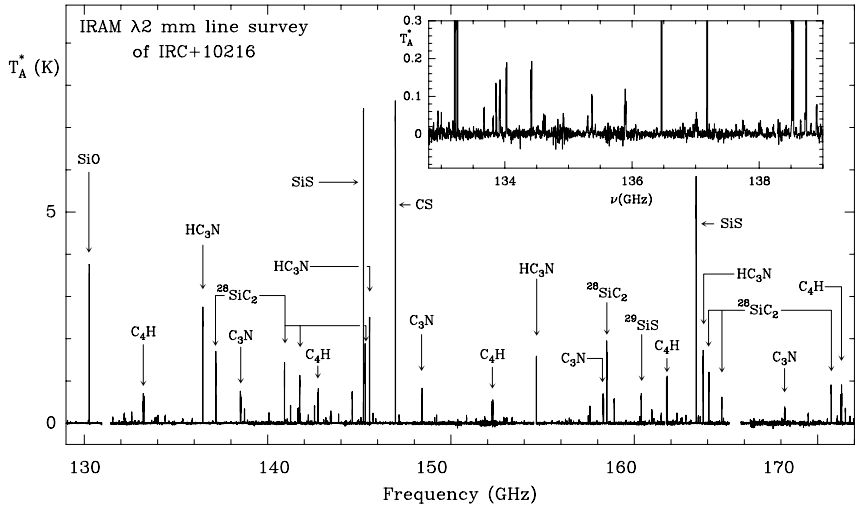

Fig. 1. The λ 2 mm IRAM 30-m telescope spectral survey of IRC+10216. The data has been smoothed to a resolution of 3 MHz ($\simeq$ 10 km s^{-1}). The spectrum is dominated by the lines of seven species: CS, SiS, SiO, SiC_2, C_4H, C_3N, and HC_3N The ordinate scale is T_A^*, the antenna temperature, corrected for spillover losses and atmosphere attenuation. The inset zooms the spectra between 132.8 and 139 GHz

Our survey was made with the IRAM 30-m telescope, the telescope with the largest effective area throughout this window.

2. Observations and data reduction

2.1. Observations

The observations were carried out between 1986 and 1997. The 2-mm SiS mixer receiver was generally optimized for the lower sideband (LSB) with an attenuation of the upper sideband (USB) between 3 and 20 dB. Rejections ≤ 6 dB were used at the high end of the surveyed band ($\nu > 160$ GHz) where the receiver could not be tuned single-sideband (SSB), and at a number of frequencies where the receiver was found to be less stable. The image rejection was measured by injecting lines in the upper and lower sidebands; this procedure is accurate to ~ 3 dB and could lead to significant calibration errors for low rejections of the image side band. Most observations were made in the balanced wobbler-switching mode, with a wobbling period of 0.5 Hz and a beam throw of $\pm 2'$. The telescope pointing and focus were checked every two hours through azimuth-elevation cross scans on the nearby continuum source OJ 287, or directly on IRC+10216 by observing centrally peaked lines, like SiS, and SiO. The system noise temperature varied between 250 K and 1000 K, depending on the observed frequency, the weather, and the source elevation.

The spectra in Figs. 1 and 2 are in units of antenna temperature, $T_{\rm A}^*$, corrected for atmospheric absorption and spillover losses (see, e.g., Cernicharo 1985). $T_{\rm A}^*$ is related to the main beam-averaged brightness temperatures by the relation $T_{\rm A}^* = B_{\rm eff}/F_{\rm eff} T_{\rm MB}$, where $B_{\rm eff}/F_{\rm eff}$, the antenna main beam efficiency, varies between 0.65 at the low end of the spectral window and 0.55 at its high end. In view of the various calibration uncertainties discussed below, we have rounded off $B_{\rm eff}/F_{\rm eff}$ to 0.6 throughout the entire band.

Most spectra were observed with a filterbank consisting of 512 two–pole filters, with halfpower widths and spacings equal to 1.0 MHz. Half a dozen of spectra were observed with an autocorrelator or with an AOS spectrometer with half-power channel-widths of 1.25 MHz; a few strong lines were observed with a 100 kHz resolution. A baseline of order 1–3 was subtracted from each 0.5 GHz–wide spectrum, after all noticeable spectral lines had been blanked out.

2.2. Determination of the line parameters

The 2-mm spectral survey extends almost continuously between 129 GHz and 172.5 GHz. Because of the limited USB rejection, the raw spectra include lines originating from both receiver sidebands. The IF center frequency being 3.932 GHz, overlapping LSB and USB lines have frequencies differing by 7.8 ± 0.5 GHz — the exact value depending on their location in the IF band. Since all spectra were observed with two or more settings of the local oscillator frequency, each line appeared at least twice in the IF band, so that its frequency could be unambiguously determined. Using our own molecular rotational transition catalog, which includes the transition frequencies of most molecules of astrophysical interest, we were able to identify the vast majority of the 380 lines we observed. One third of those were assigned to astrophysical species which were unknown at the time we started our survey. One sixth of the lines remain unidentified. The detected lines, ordered by frequency, and their assigments are listed in Table 2. The unidentified lines are summed up in Table 3.

Depending on their apparent shapes, the line profiles were fitted with the cusped, flat, or parabolic profiles expected from optically thin/thick lines arising in a uniformly expanding spherical shell (see Morris 1985). The expansion velocity, $V_{\rm exp}$ and the systemic velocity $V_{\rm sys}$, were derived through fits to the strongest lines. They were found to be the same for all lines, $V_{\rm exp} = 14.5 \pm 0.2$ km s^{-1} and $V_{\rm sys}$(LSR) $= -26.5 \pm 0.3$ km s^{-1}, except in the cases of the vibrationally excited lines of SiS and CS which arise in the hot region close to the star.

Tables 4–9 present the fitted transitions and line parameters, ordered by molecular species and isotopomer. As explained in Sect. 2.1 the integrated main beam brightness temperatures, $T_{\rm MB}$, are related to antenna temperatures (the units of Figs. 1 and 2) through the formula $\int T_{\rm MB} {\rm d}v = F_{\rm eff}/B_{\rm eff} \int T_{\rm A}^* {\rm d}v$.

2.3. Calibration and removal of USB lines

In order to properly calibrate the intensity scale, many strong lines were re-observed with a high rejection of the image side band (≥ 17 dB). The intensity of these "primary" calibrators was used to calibrate the lines > 0.3 K appearing in the same spectra. Those lines, in turn, were used to calibrate more distant lines. Because of the large number of overlapping spectra, it was possible to calibrate with three such steps one $2-3$ GHz-wide band around each "primary" line. The intensities of the lines at the intersection of two such bands were typically found to be consistent within 10%. We note, however, that we have assumed a constant rejection of the image signal across the IF band. This may not be true at some frequencies, and could in exceptional cases lead to larger calibration errors. Finally, because of the higher atmospheric attenuation and of the low image side band rejection above 160 GHz, the calibration uncertainty raises to $10-25\%$ between $160-172.5$ GHz.

Because each portion of our spectral scan is the average of several LSB spectra, observed with different settings of the LO, any line from the USB improperly rejected will

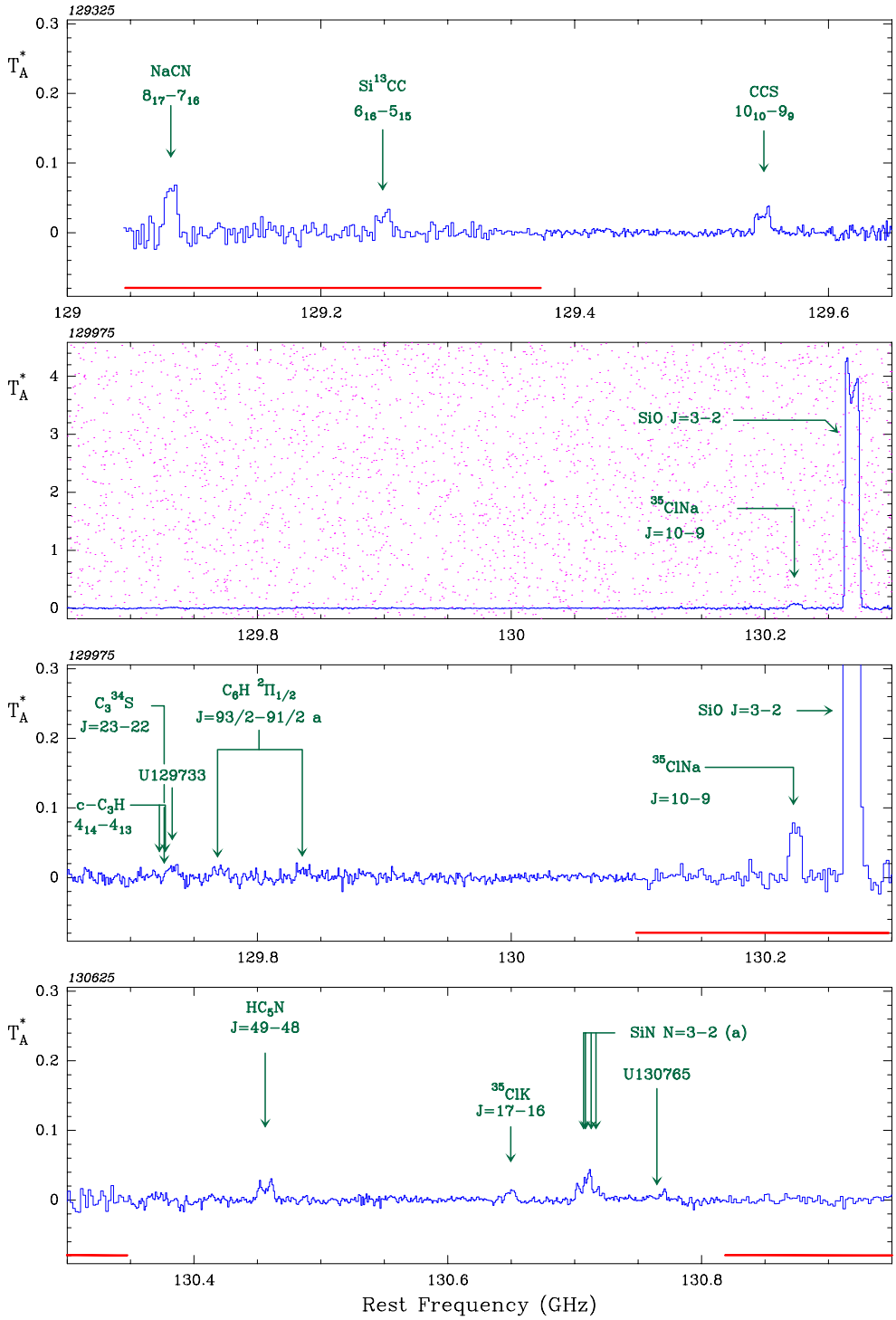

Fig. 2. The λ 2 mm spectral survey of IRC+10216 at a full resolution. The spectral resolution is 1 MHz, except in the intervals marked by an horizontal dotted line, where it is 2 MHz (see text). Ordinate is T_A^*, the antenna temperature corrected for atmosphere absorption and spillover losses. This latter is related for to the main beam-averaged brightness temperatures by the relation $T_{A*} = B_{eff}/F_{eff} T_{MB}$, where B_{eff}/F_{eff} is the antenna main beam efficiency. The spectra are drawn at the scale $-0.1 < T_A^* < 0.3$ K, except for those with peak temperatures between 0.3 and 0.5 K which are drawn at a slightly smaller scale (they are marked with a black square on the top right corner). In addition, the spectra with lines > 0.5 K are redrawn at full scale (marked with a dotted background). Note that most lines exhibit cusped profiles with full width 29.0 km s^{-1}

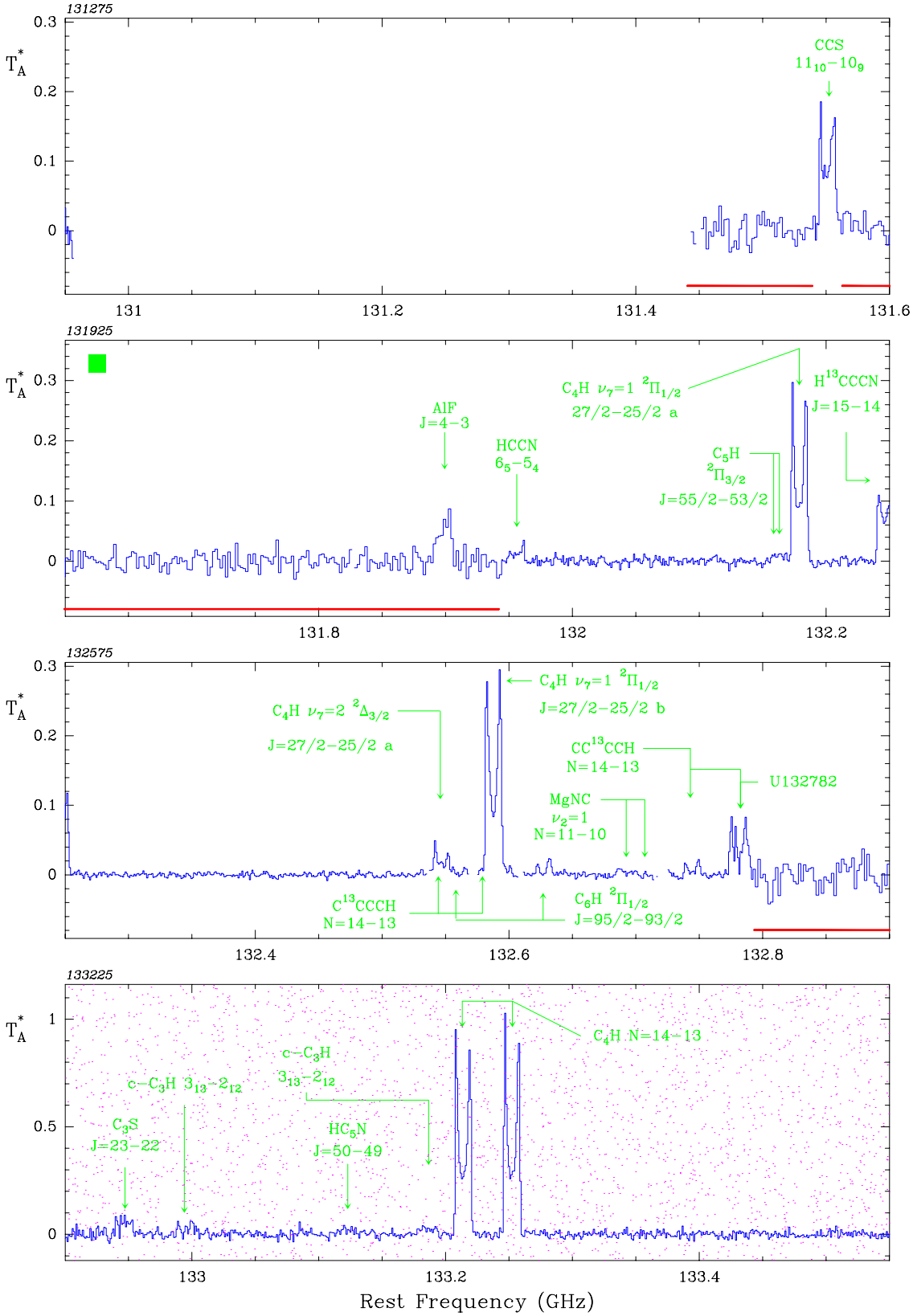

Fig. 2. continued

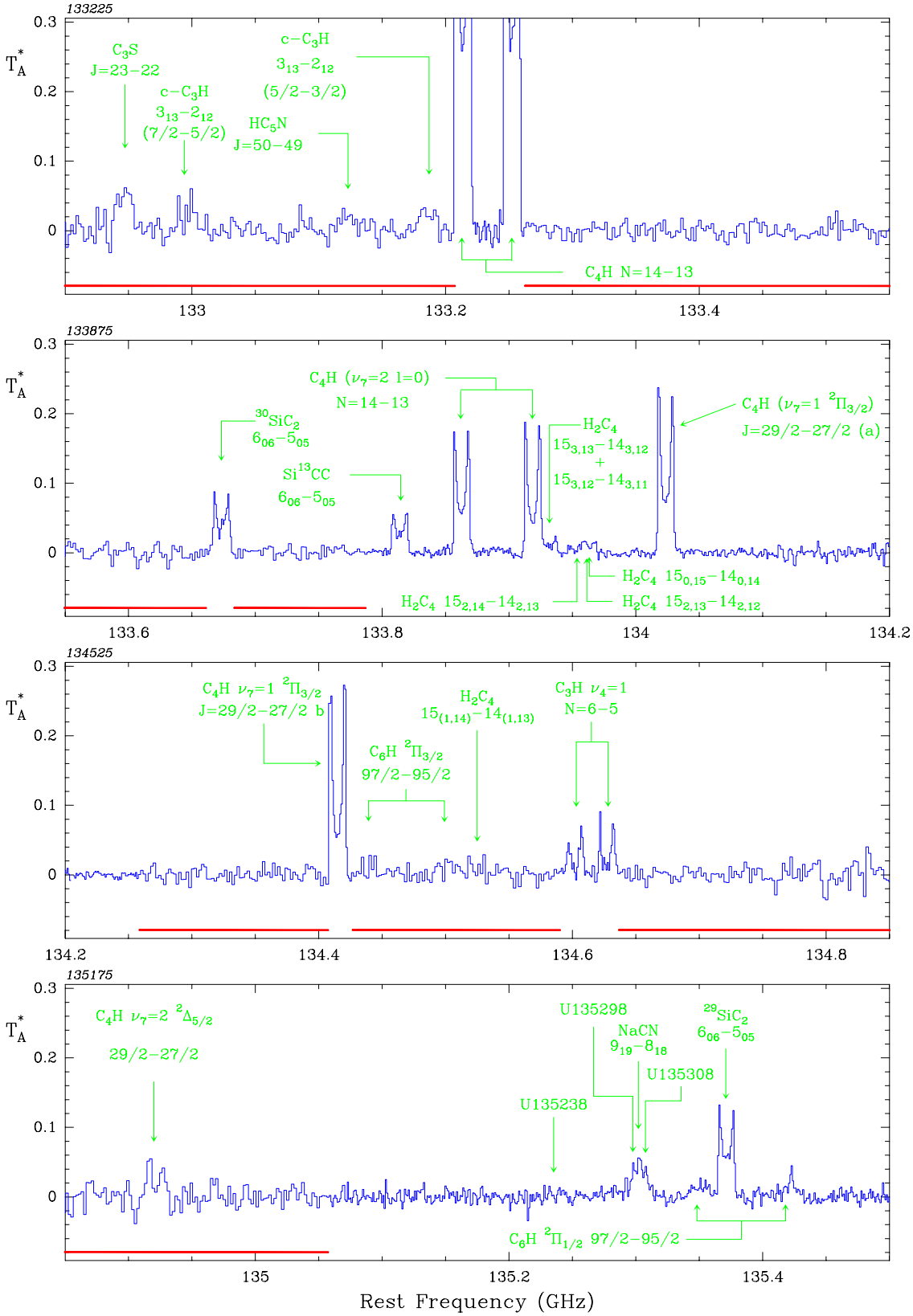

Fig. 2. continued

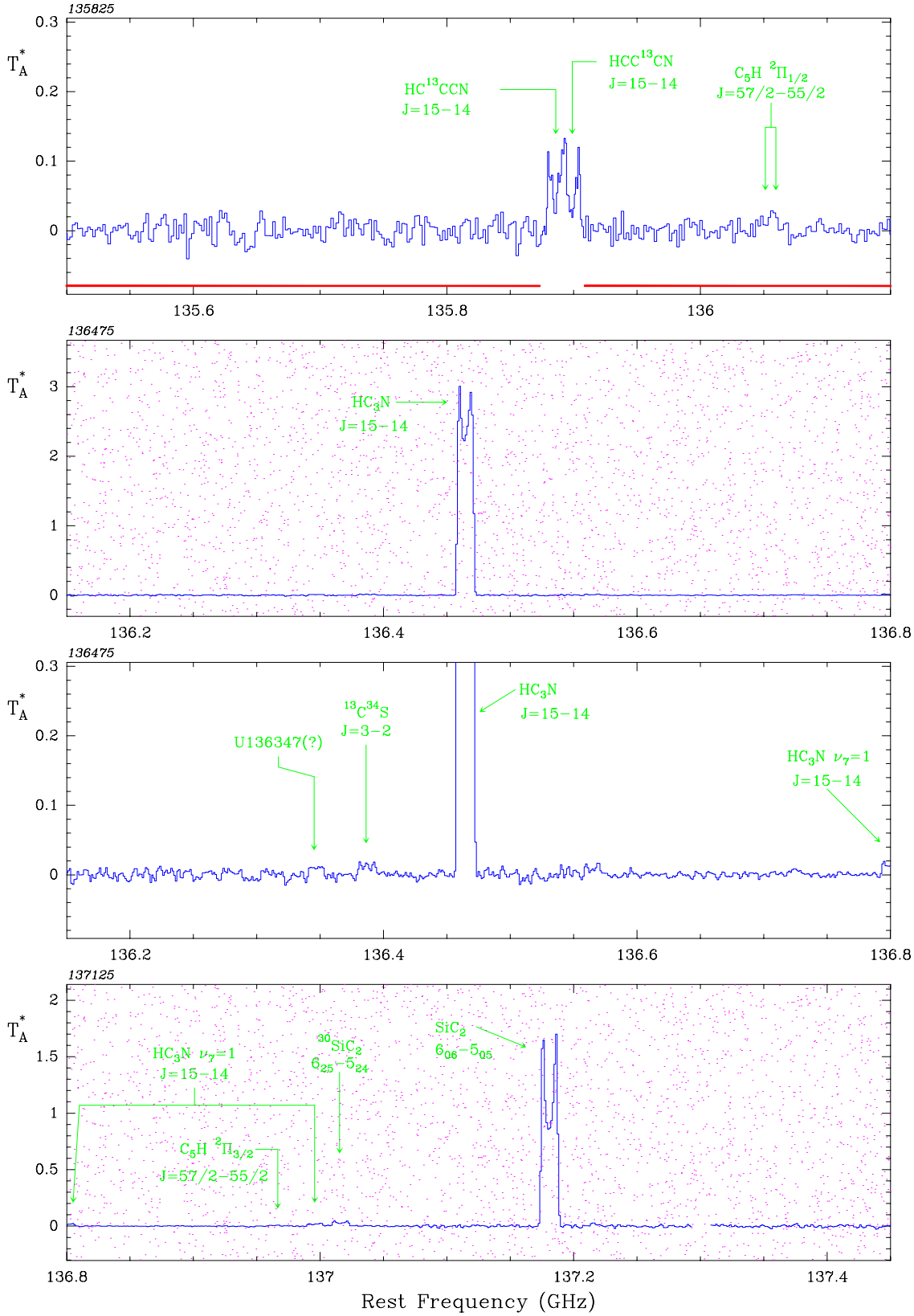

Fig. 2. continued

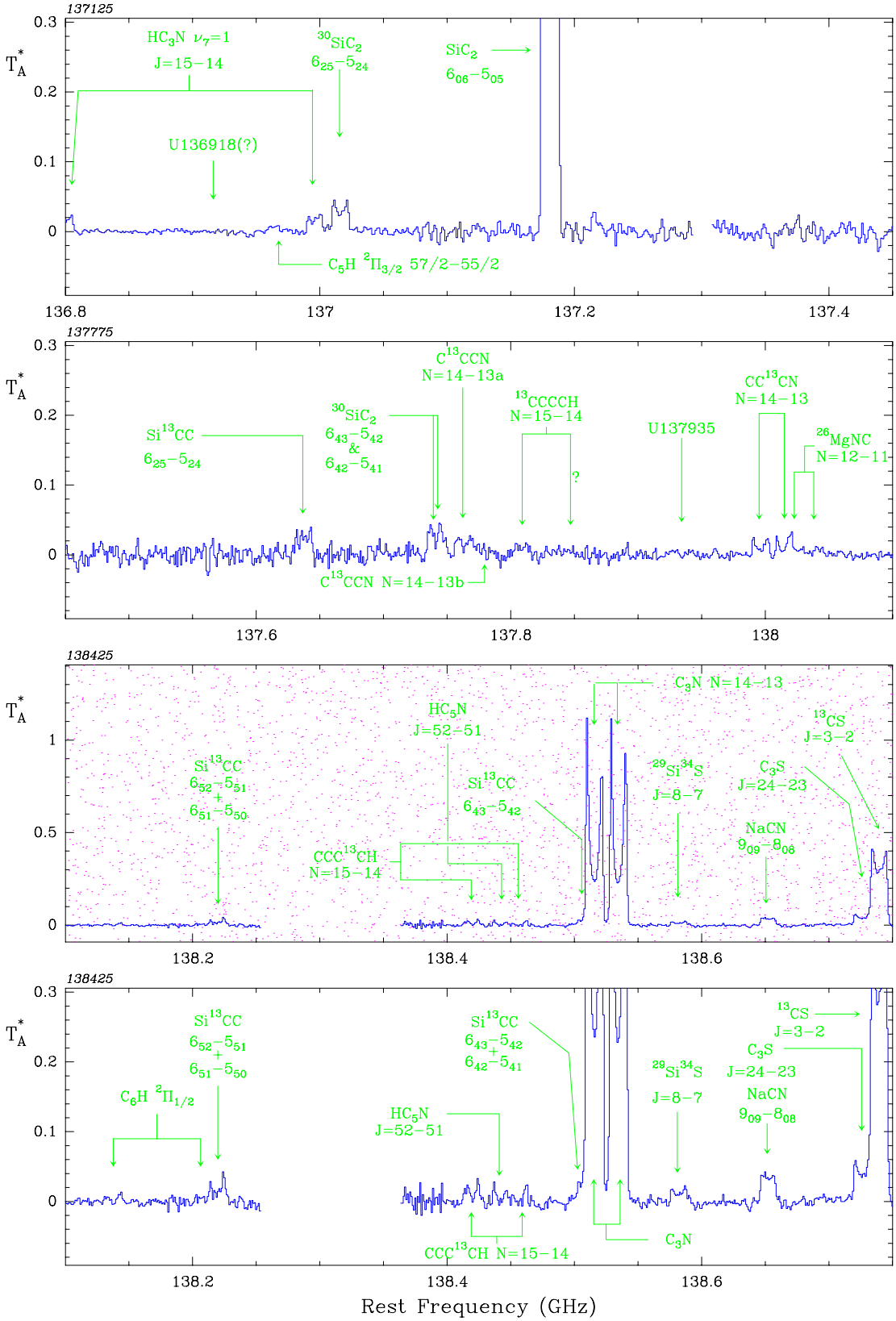

Fig. 2. continued

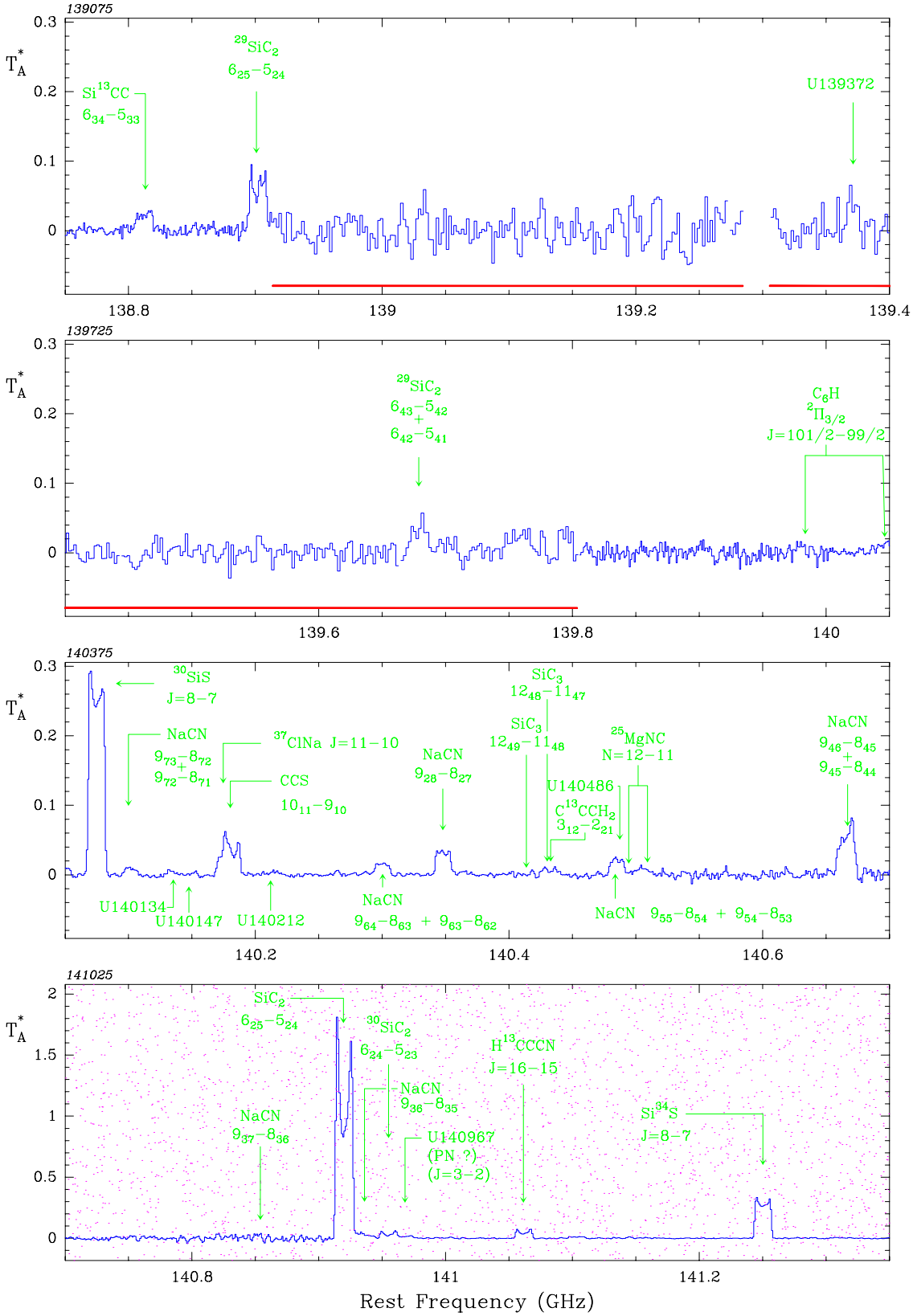

Fig. 2. continued

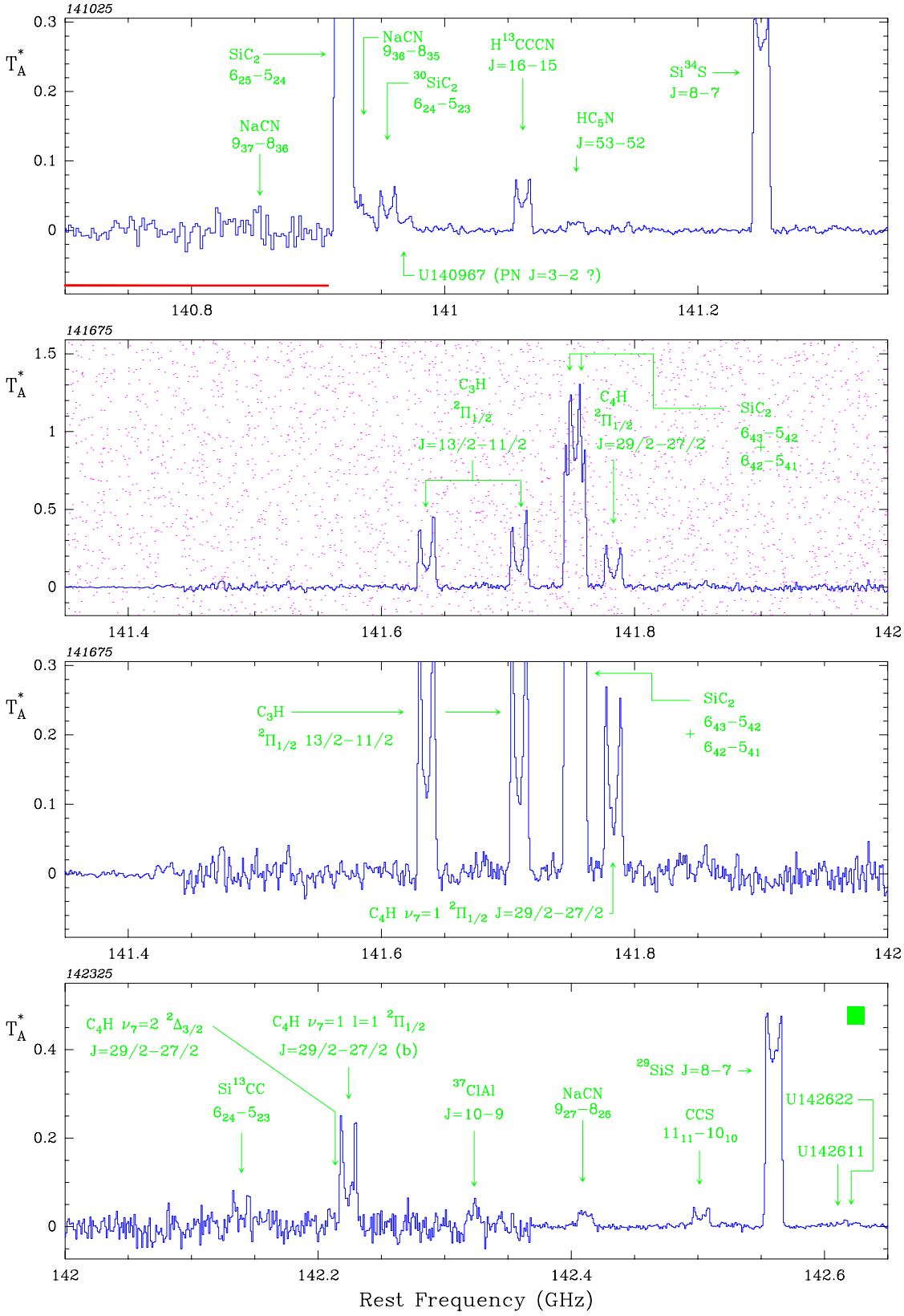

Fig. 2. continued

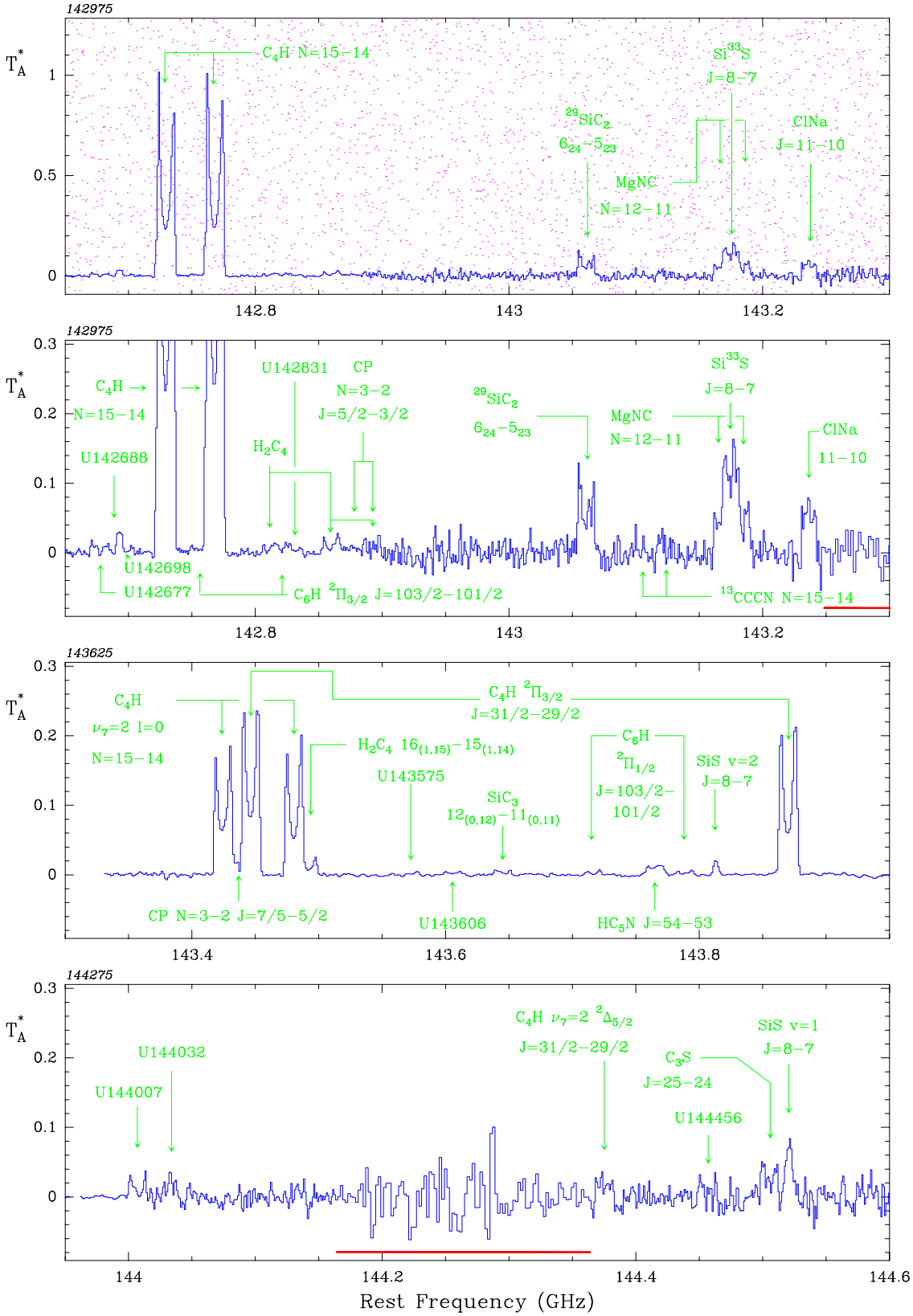

Fig. 2. continued

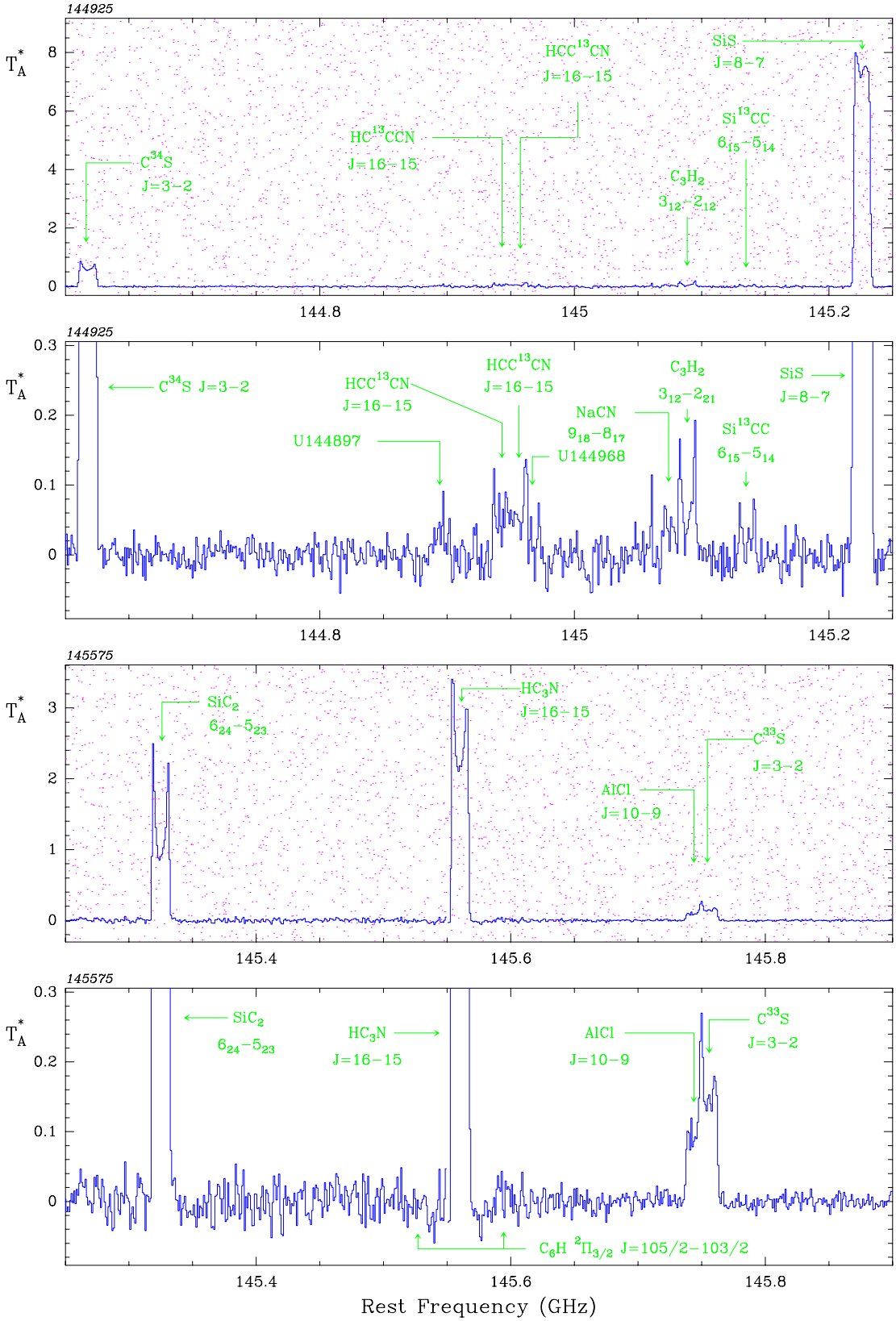

Fig. 2. continued

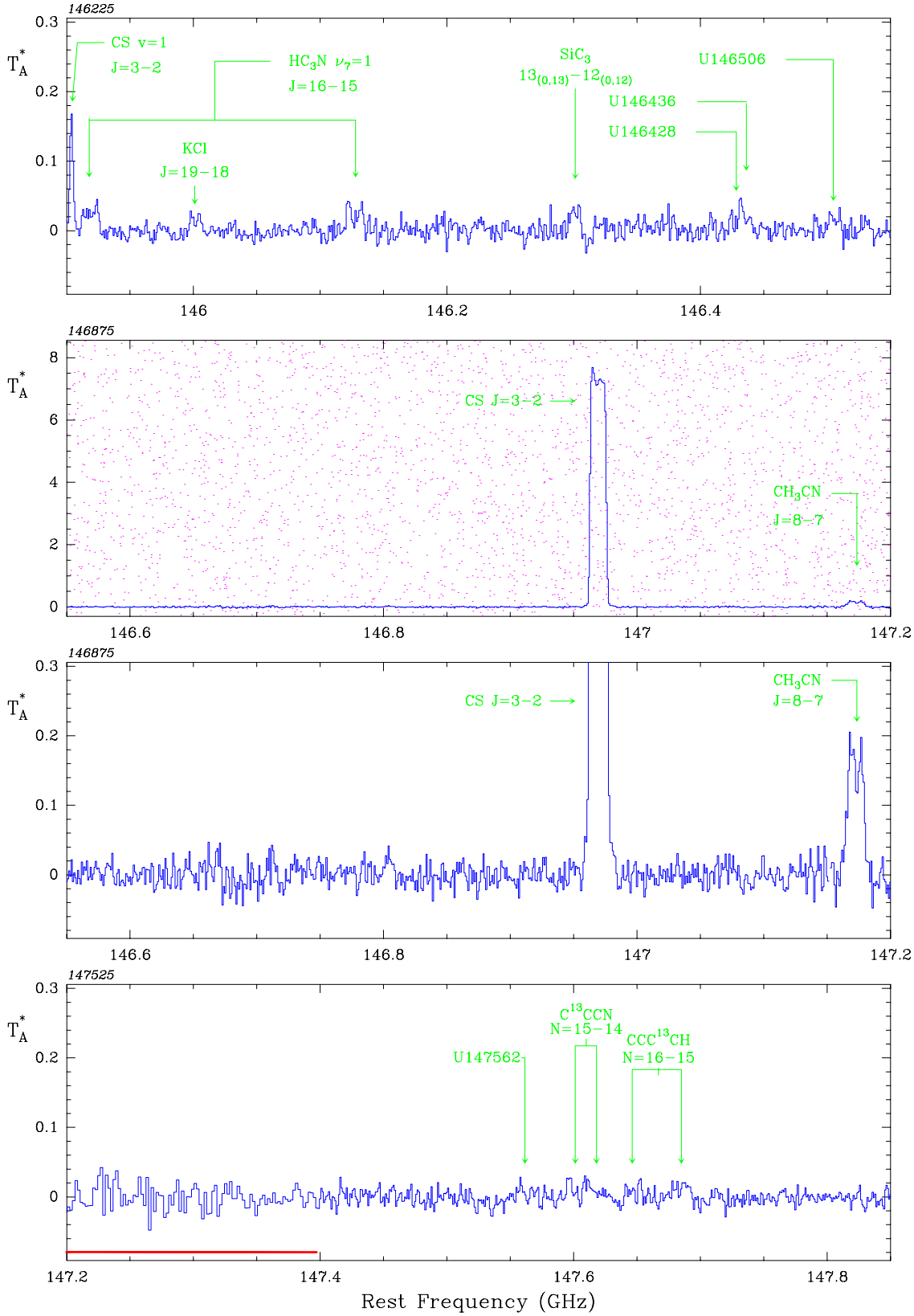

Fig. 2. continued

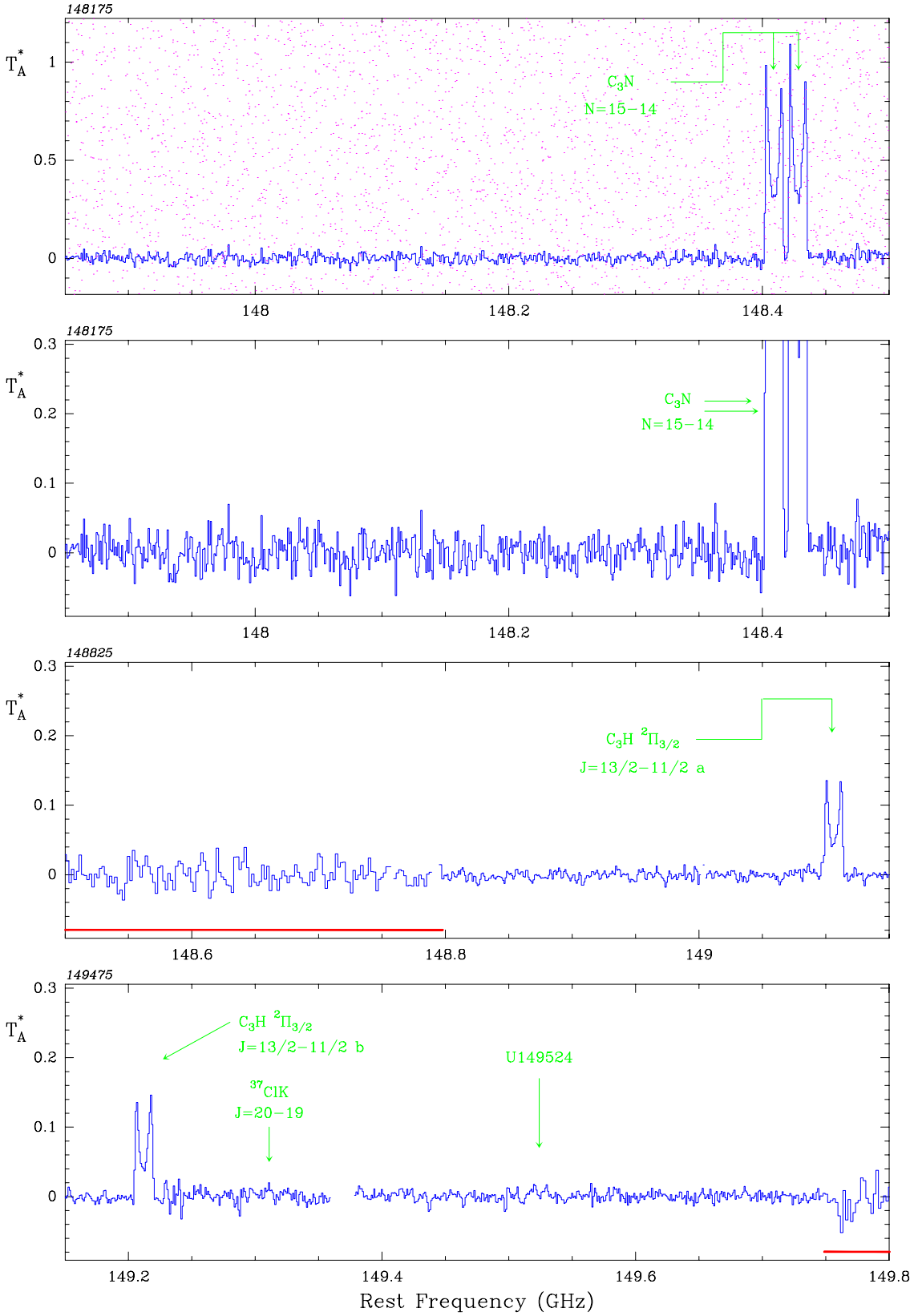

Fig. 2. continued

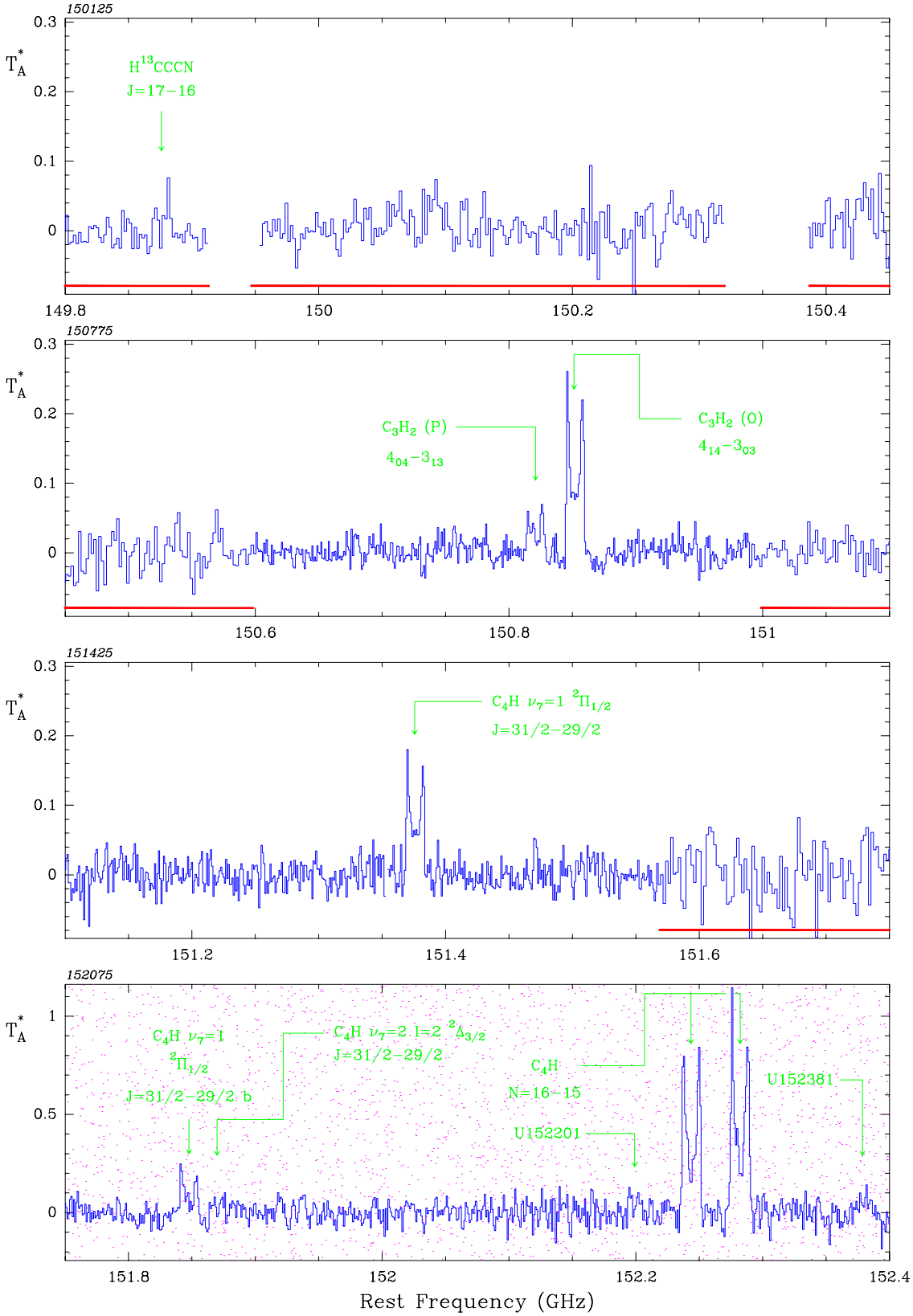

Fig. 2. continued

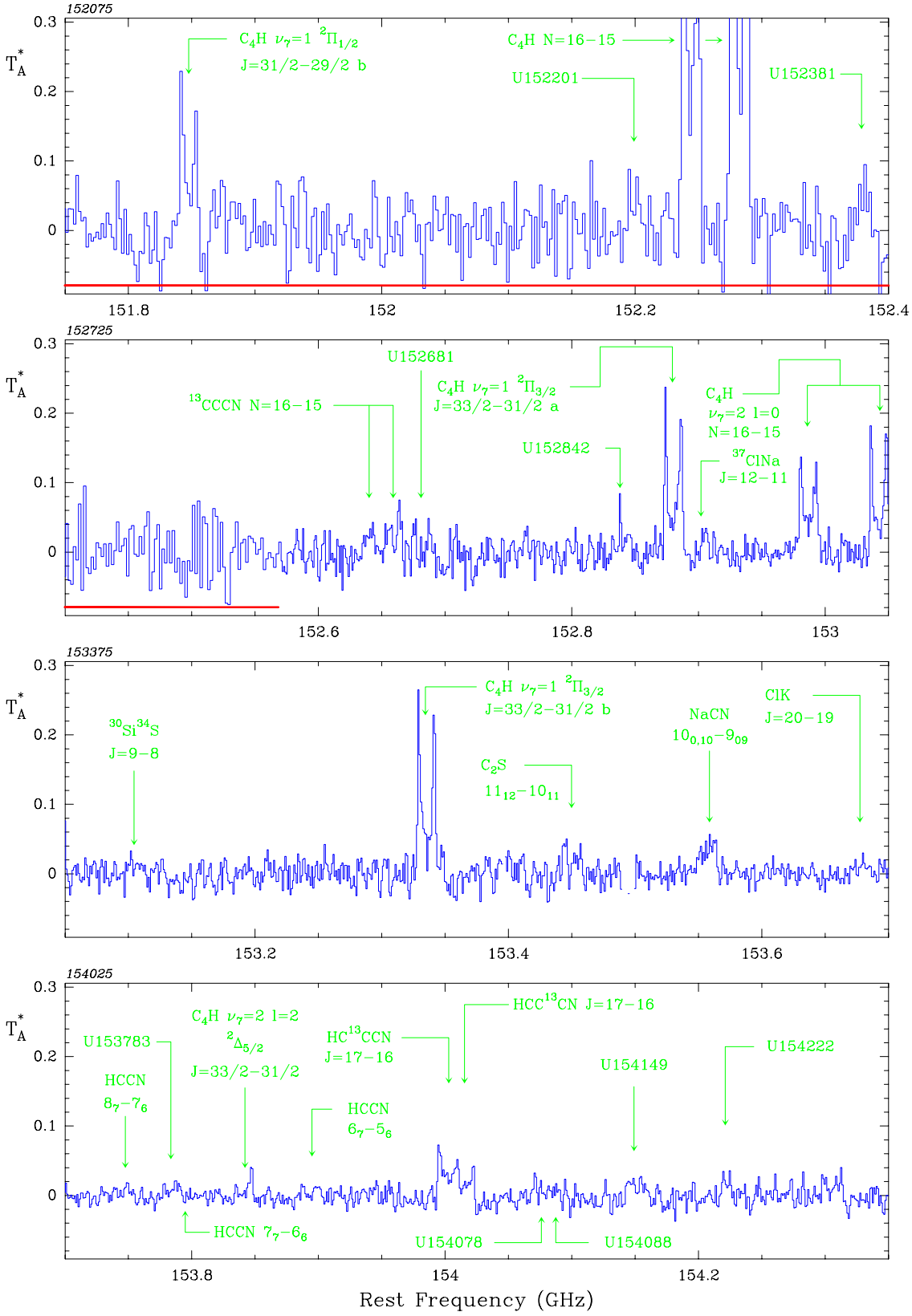

Fig. 2. continued

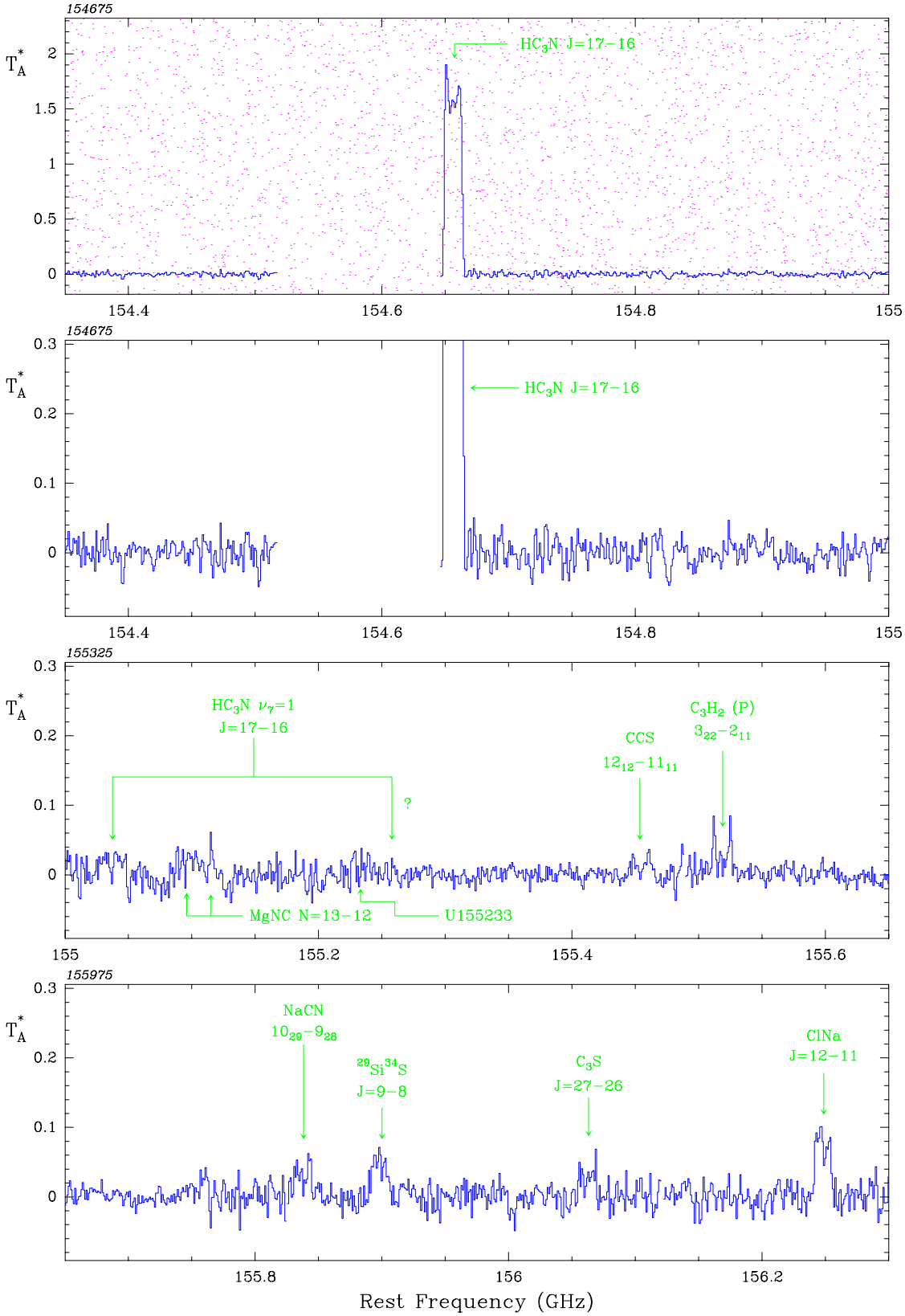

Fig. 2. continued

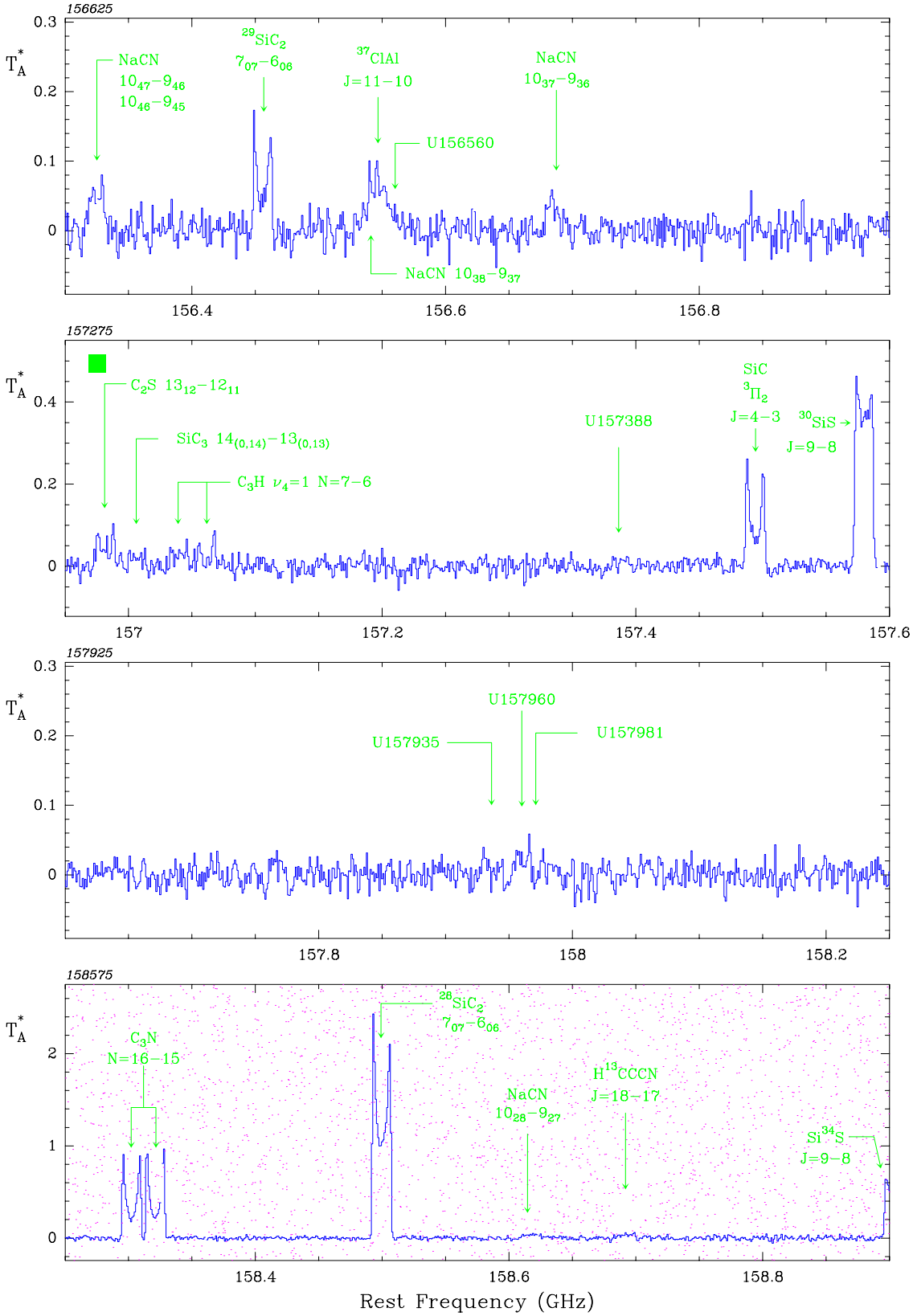

Fig. 2. continued

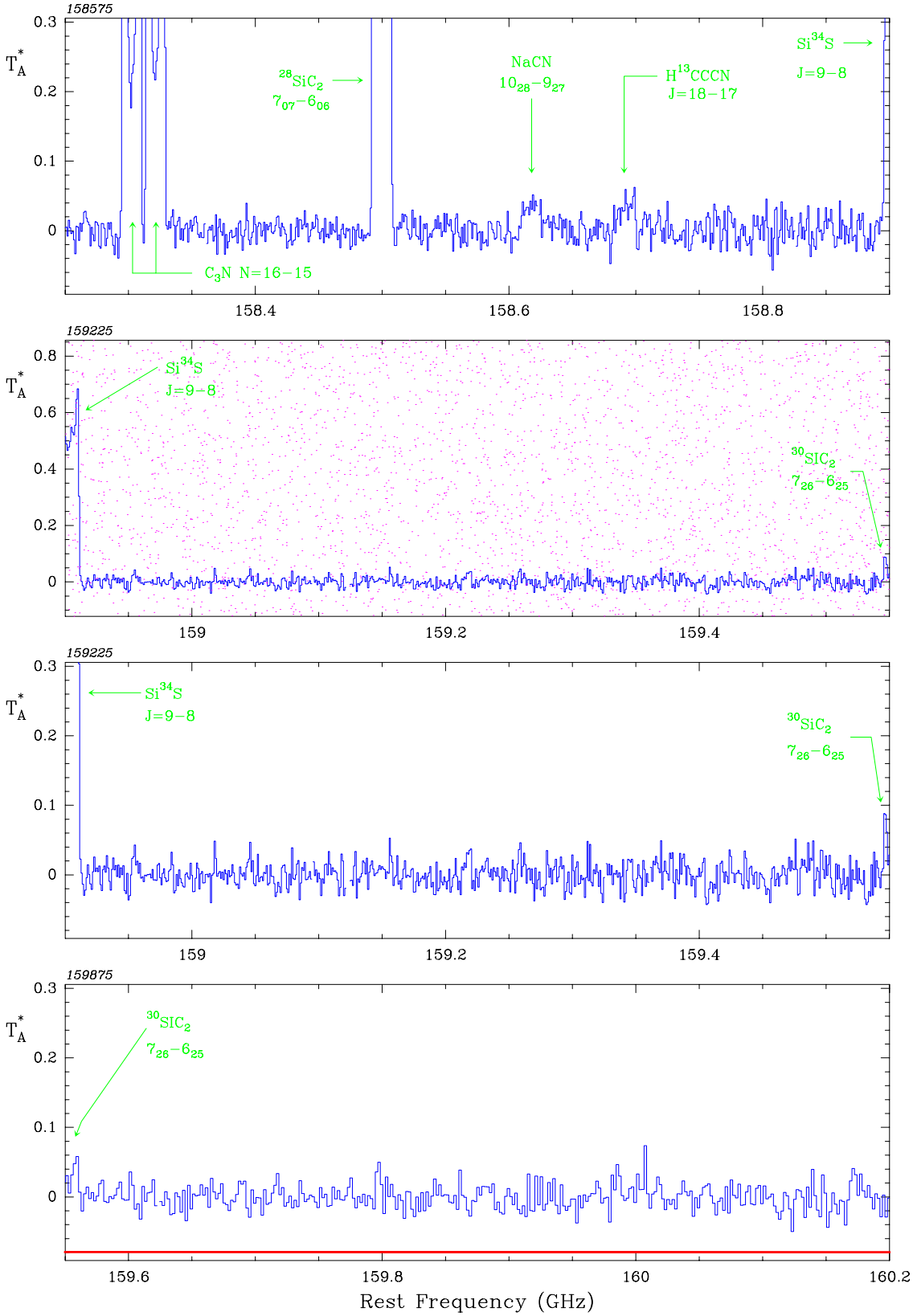

Fig. 2. continued

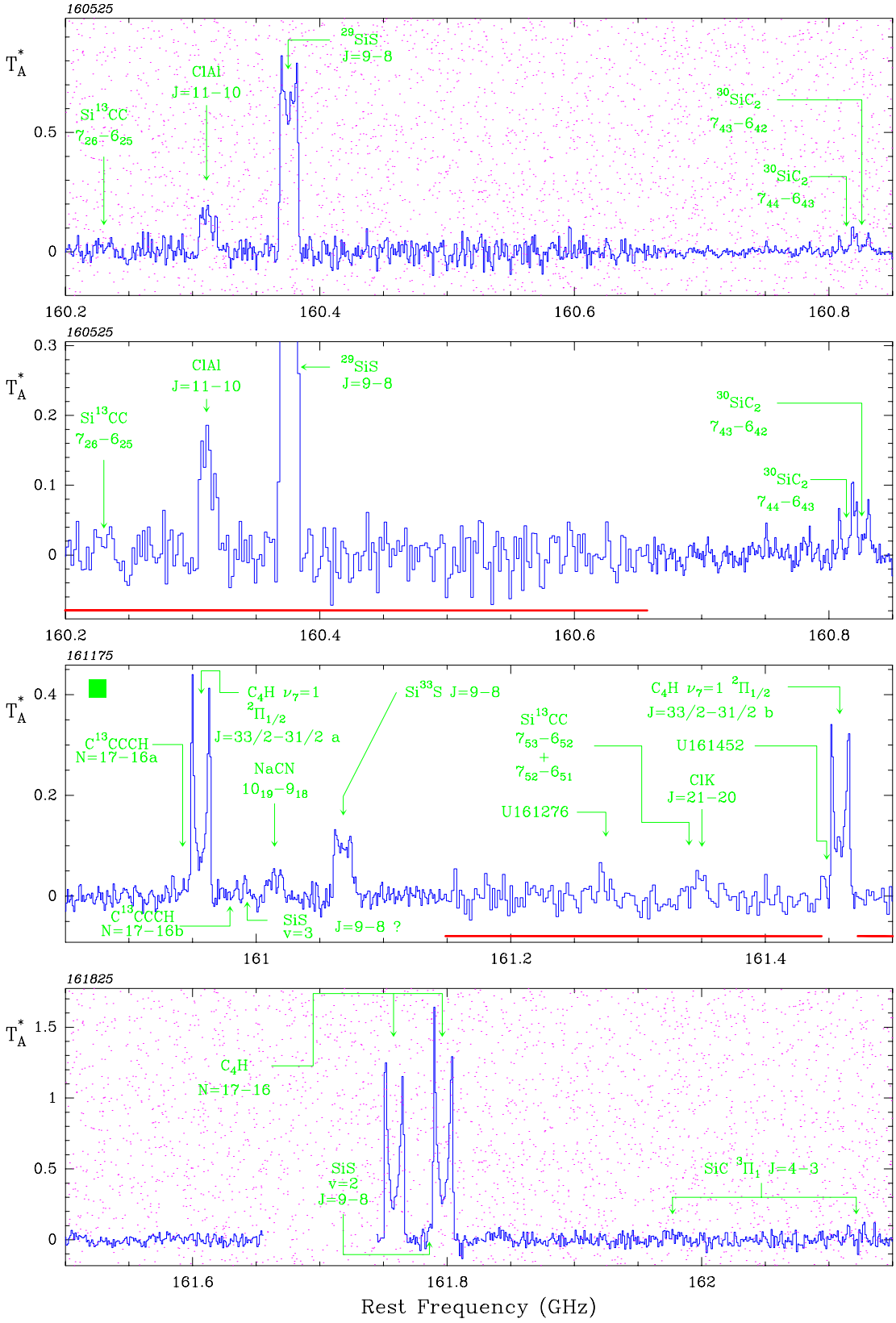

Fig. 2. continued

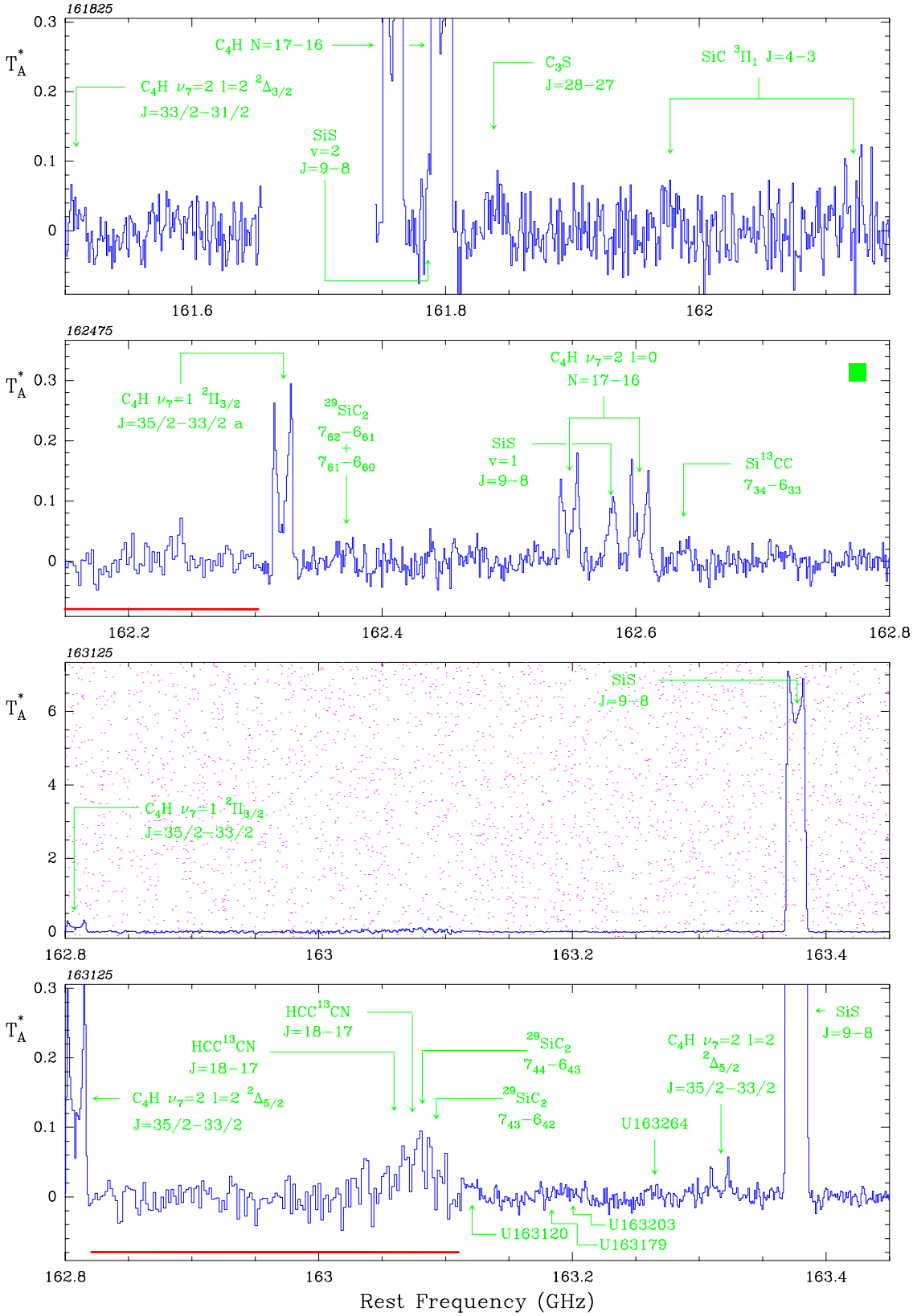

Fig. 2. continued

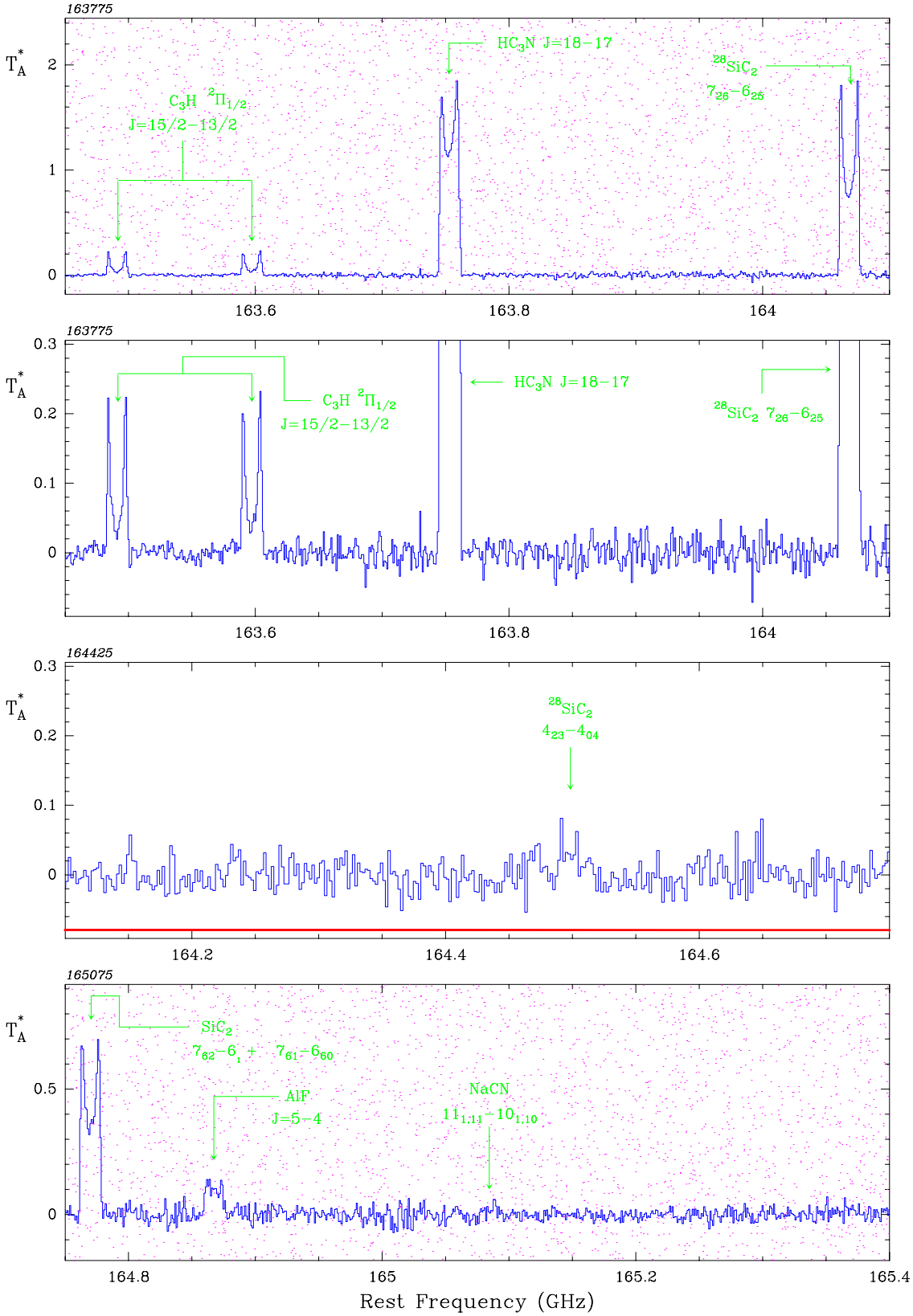

Fig. 2. continued

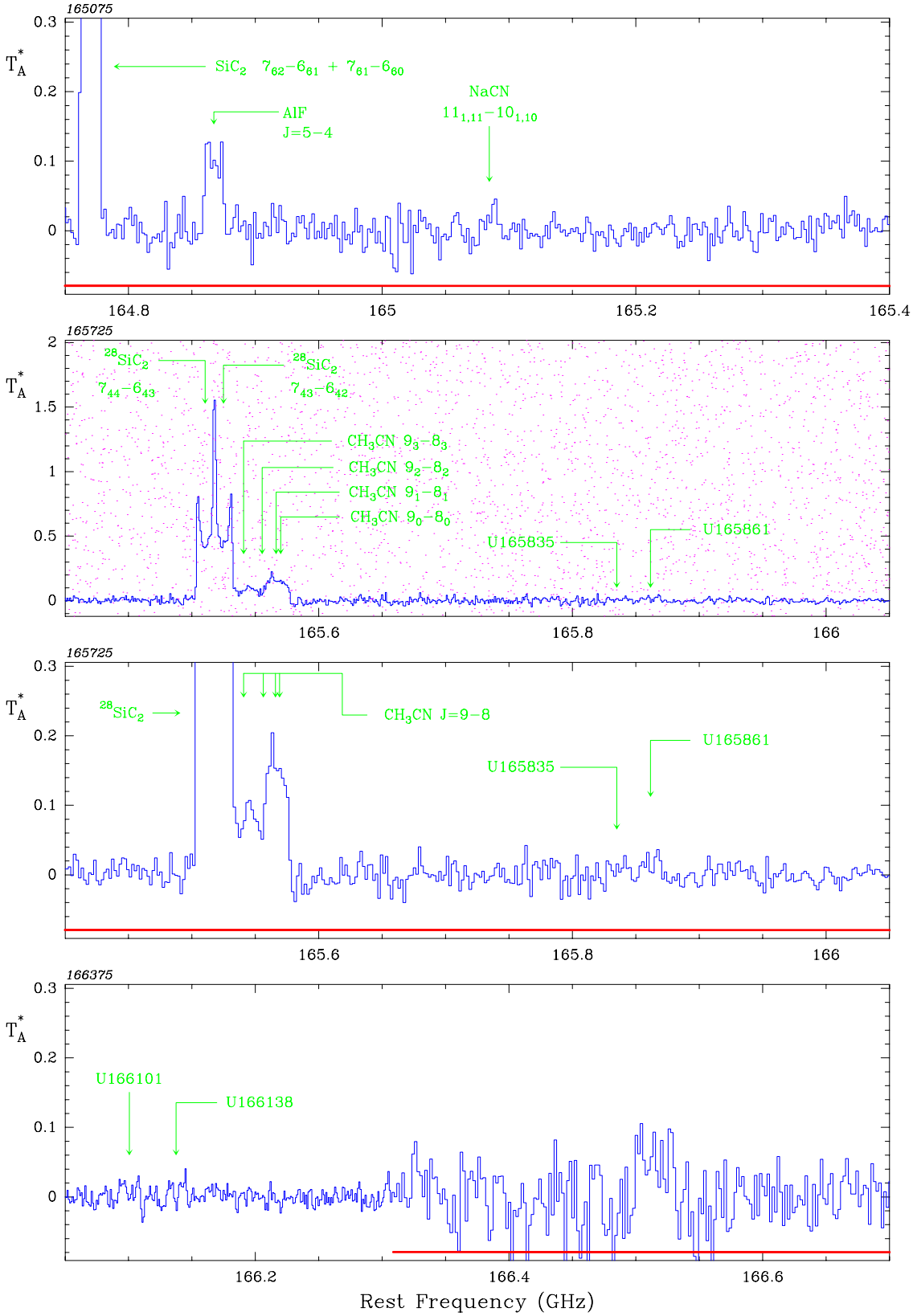

Fig. 2. continued

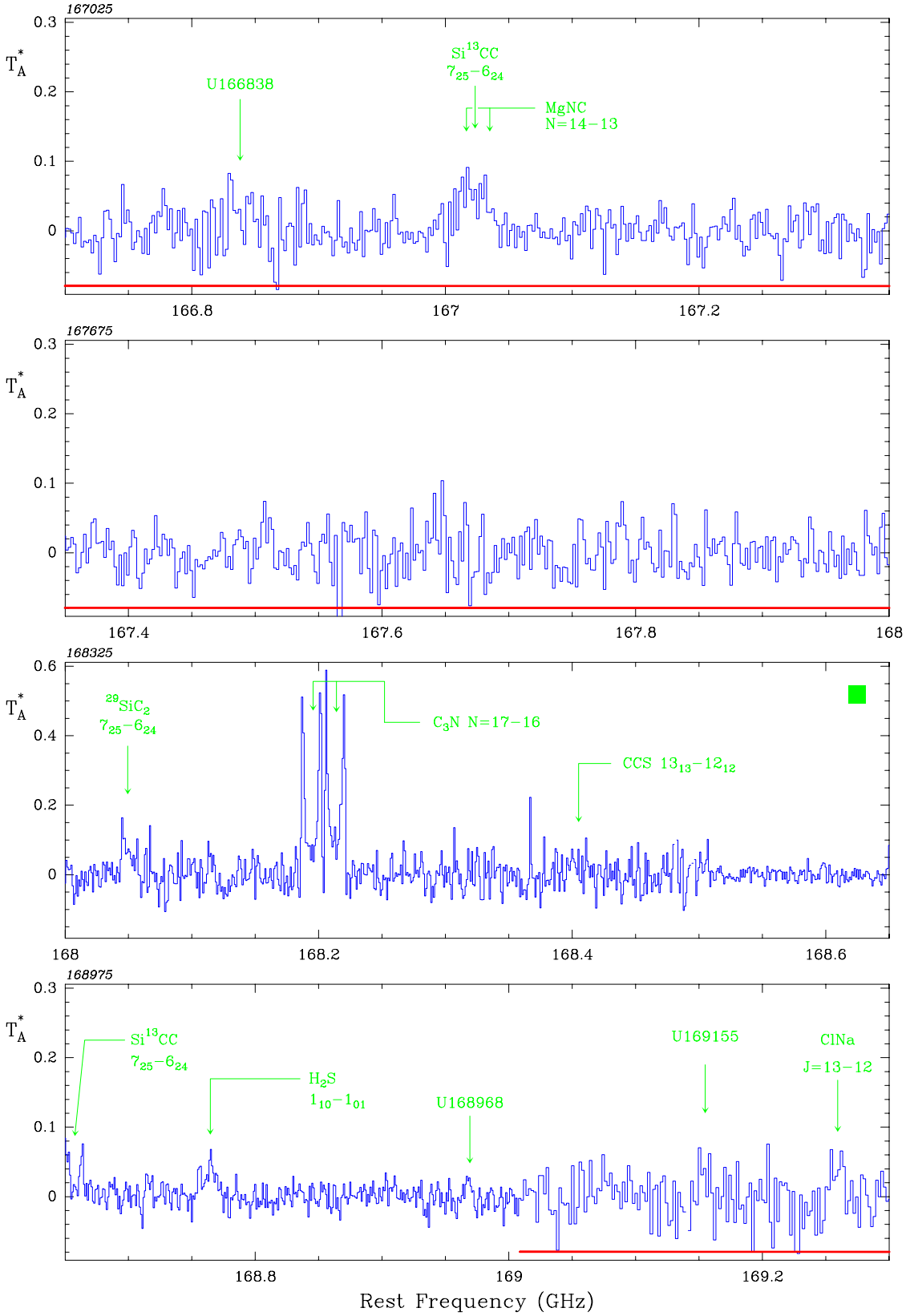

Fig. 2. continued

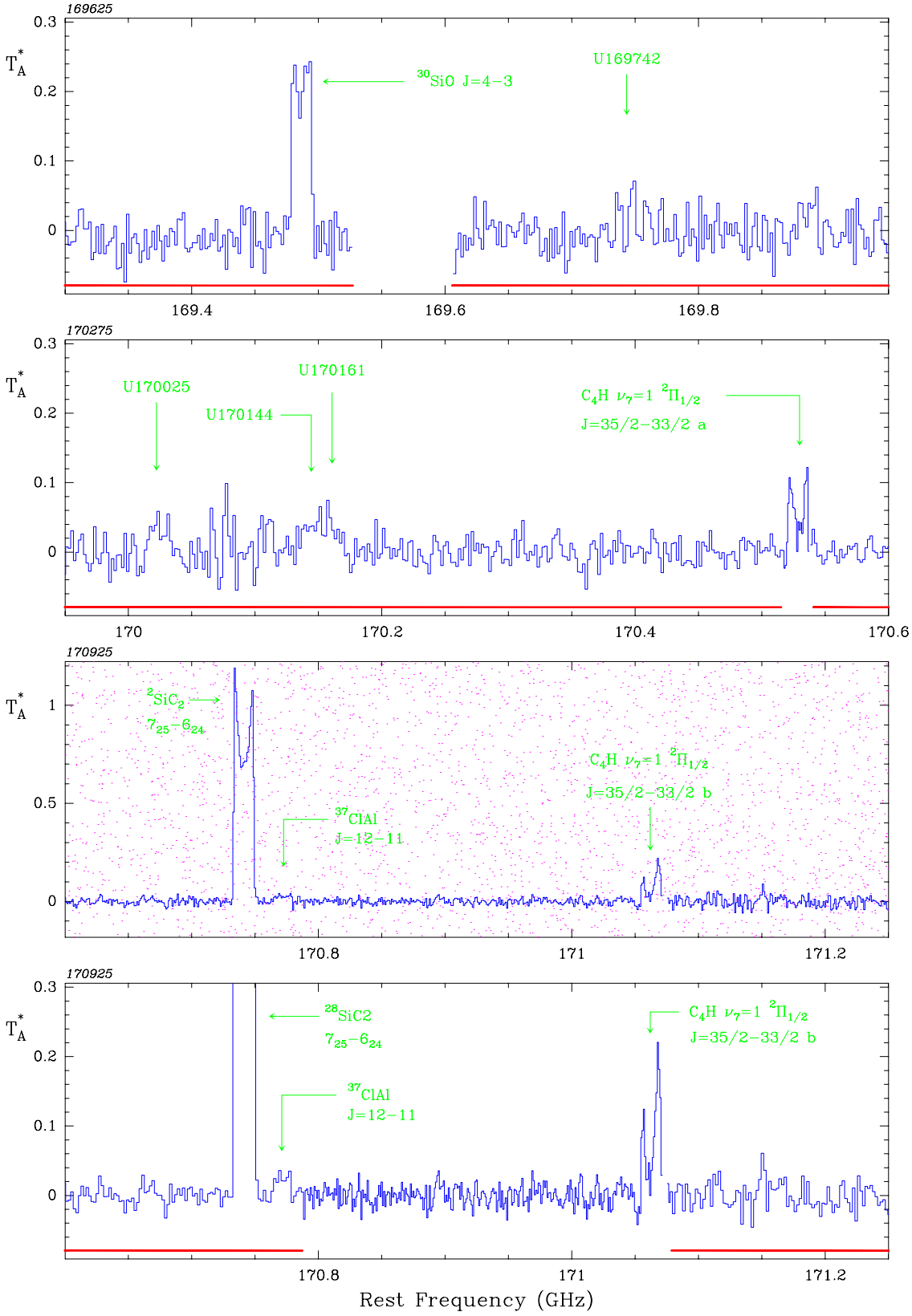

Fig. 2. continued

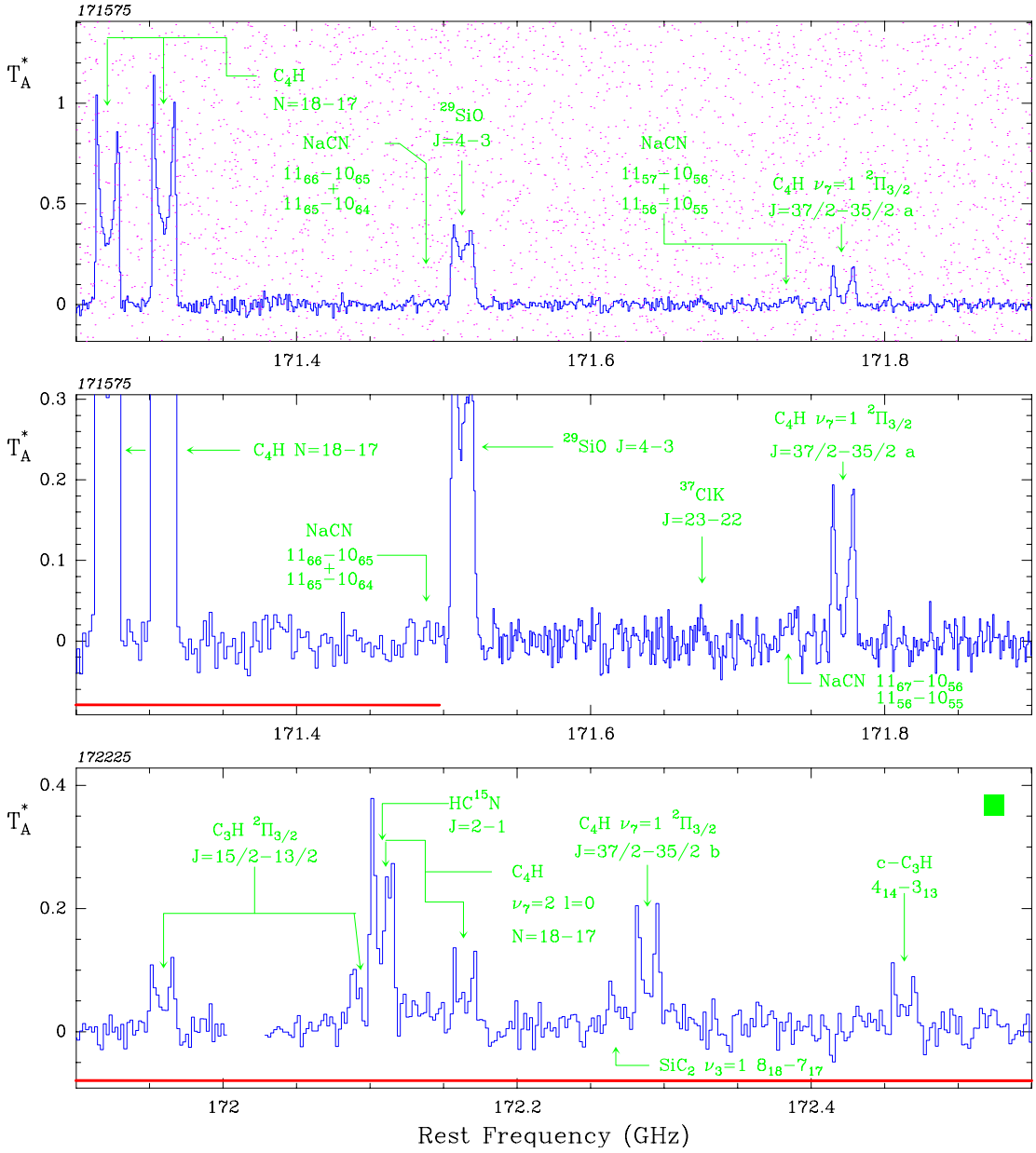

Fig. 2. continued

appear at several locations in the average spectra. The resulting ghosts of USB lines would then be difficult to trace out and identify. All traces from USB lines have thus to be removed prior to averaging the original spectra, which was done in the following way:

i) USB lines were first identified from a comparison of overlapping spectra observed with different LO settings and/or by an inspection of the portion of the spectral scan 8 GHz higher in frequency. *ii)* In the case of weak ghosts (i.e. when the USB lines were weak or the USB rejection was high), we fitted to the USB ghosts theoretical profiles, whose shape, frequency, and width were derived whenever possible from the high frequency spectra. Then *iii)* we subtracted the fitted profiles from the original spectrum. *iv)* In the cases of strong USB ghosts, or of severe blending between USB and LSB lines, the channels covered by the USB ghost were simply blanked out.

The spectra processed in this way were averaged and combined yielding a first version of the 42 GHz-wide spectrum. Processes *i)* to *iv)* were then repeated to yield a second version, then a third version of the complete spectrum. We performed five such iterations to make sure that all remaining spectral features are lines from the signal sideband.

We note that the re-calibration of the spectra and the elimination of USB lines was greatly eased by the complete coverage of our survey: the line intensities we previously published from the analysis of individual

spectra are a priori less reliable than those reported in this work.

2.4. Time variability

IRC+10216 is known to be a Mira-type variable with a periodicity of 1.71 yr. Its 10 μm flux varies by a factor of 2 between minimum and maximum. Because of the calibration method described above, it was important to check for time-related intensity variations. Depending on the relative importance of radiative and collisional excitation, the millimeter line intensities may or may not follow the infrared flux variations. Among the 2-mm lines, the most likely to be affected are: *i)* those of CS, HC_3N, SiO and SiS, four species whose IR lines are known to be optically thick, as well as *ii)* the vibrationally excited lines of C_4H and HCN (Lucas & Cernicharo 1989). These lines were observed at several occasions during the 10 yr-long observing period. The ground-state mm lines, observed at a resolution of $\simeq 2$ km s^{-1}, were found to have stable shapes and intensities (within 20% which is consistent with our calibration uncertainty). The $v = 1, J = 3 - 2$ line of CS and several mm lines of vibrationally excited C_4H were observed with a good signal-to-noise ratio at different IR-phase periods in the course of our survey. We saw no intensity variations $> 20\%$ which could be correlated with the IR flux phase. However, the strong $\nu_2 = 1, J = 2 - 1$ line of HCN near 177 GHz shows factor of 2 intensity variation with time; this line, however, is known to be masering (Lucas & Cernicharo 1989).

Intensity comparisons are more difficult for weaker lines. We can only quote an upper limit of 20%, which represents the scatter of the intensities recorded at different epochs for the $0.3 - 0.5$ K lines. Most of this scatter is probably related to calibration errors, since we found no obvious relation with the IR flux variations.

3. Analysis of the spectral survey

3.1. Line identifications

Figure 1 shows an overview of the 2-mm SSB spectral survey at a resolution of 3 MHz ($\simeq 6$ km s^{-1}). The spectrum is dominated by the lines of half a dozen of species: CS and SiS whose lines have $T_{\rm MB} \geq 10$ K; SiO, SiC_2 and HC_3N with $T_{\rm MB} \geq 5$ K; C_3N and C_4H with $T_{\rm MB} \geq 1$ K. Figure 2 shows the survey at full spectral resolution. The ordinate scale is antenna temperature, corrected for rear sidelobes and atmosphere attenuation. Most spectra are plotted at a fixed intensity scale ($-0.1 - 0.3$ K).

There are 380 spectral lines visible in Fig. 2. Their rest frequencies and intensities are given in Table 2. 83% of these lines can unambiguously be assigned to known molecular species; 63 lines (denoted by the letter U) remain unidentified.

While the 2-mm spectrum of IRC+10216 seems now well understood, such was not the case when we started our observations. Only SiO, SiS, H_2S, HC_3N, HC_5N, C_3N, C_3H, C_4H, and SiC_2 were known to have lines in the 2-mm window. As a matter of fact, the first goal of our survey was to search for metal-bearing compounds and for SiC, whose spectroscopic parameters were poorly known.

In 1987, after the first half of the survey had been completed, we realized that most of the 2-mm lines in IRC+10216 were not visible in the spectra of Orion A or Sgr B2 and that 4 out of 5 lines could not be assigned to any known astrophysical molecule. There followed a several year-long effort to identify the carriers of these unidentified lines. We searched for line patterns characteristic of linear carbon chains, such as the harmonically related series of doublets which led to the discoveries of MgNC, C_5H, and vibrationally excited C_4H (Guélin et al. 1986; Cernicharo et al. 1986a,b, 1987a,b; Guélin et al. 1987a), and determined the inertia moments of the carriers. Knowing that IRC+10216 is rich in unsaturated C species and poor in oxygen compounds, we guessed on the basis of simple bond-length considerations, of quantum mechanical calculations, or of existing spectroscopic data what species were the most likely carriers. In many cases the avaibility of accurate rotational constants, derived from microwave laboratory measurements, left no doubt as to the identities of the carriers. In other cases (5 out of 22) the carriers were identified prior to the availability of any laboratory data.

3.2. Catalogue of lines of astrophysical interest

To help with the identification of the lines, we compiled a catalog of the mm-wave transitions of all the molecular species with known rotational constants that were likely to be abundant in IRC+10216 (Cernicharo 1988). The spectroscopic data were taken from the literature – see in particular the compilations by B. Starck & J. Vogt from Universität Ulm (Demaison et al. 1974; Vogt 1998) and by Lovas and co-workers (Lovas & Tiemann 1974; Lovas 1978, 1986), as well as the references in Poynter & Pickett (1984). In several cases, laboratory measurements were triggered by our work (see Cernicharo et al. 1986c, 1989, 1991a; Cernicharo & Guélin 1987, 1996; Gottlieb et al. 1986, 1989; Guélin et al. 1987b, 1995).

The frequencies of the rare isotopomers of a diatomic molecule can be fairly accurately derived from the spectroscopic constants of their main isotopomers. As is well known (see e.g. Gordy & Cook 1984), Dunham's molecular constants $Y_{\rm lm}$ scale with the reduced molecular mass $\mu_{\rm r}$ as

$$Y_{\rm lm} \sim \mu_{\rm r}^{-(l+2m)/2},$$

at least in the first order. Applying this relation and the standard formula expressing the rotational transition frequencies in function of the $Y_{\rm lm}$s (see e.g. Lovas & Tiemann

1974), it was possible to derive the transition frequencies of diatomic molecules from those of a parent isotopomer within few $\times 10^{-6}$. Species calculated in this way were ^{29}Si^{34}S, ^{29}Si^{33}S, ^{30}Si^{34}S, ^{30}Si^{33}S, Si^{18}O, Si^{17}O, ^{29}Si^{18}O, ^{29}Si^{17}O, ^{30}Si^{18}O, and ^{30}Si^{17}O. Some unstable isotopes of other molecular species as ^{26}AlF, ^{32}SiO, Na^{36}Cl, K^{36}Cl and Al^{36}Cl, have been also included in our catalogue.

The catalogue contains now about 560 molecular isotopomers or species and more than 1.8 10^5 lines in the range $1 - 300$ GHz. The accuracy of the predicted frequencies is better than 1 MHz for most lines.

4. Discussion

4.1. Molecular abundances

Depending on their formation processes, most molecular species observed in IRC+10216 are confined either to the inner envelope ($R \leq 6''$), or to a thin hollow shell of radius $\sim 15''$. This was discussed in particular by Guélin et al. (1993) and Guélin et al. (1997), who showed that the lines of the carbon chain radicals exhibit very similar spatial brightness distributions in spite of their different Einstein coefficients. Most metal-bearing species like NaCl, AlCl, KCl, AlF (Cernicharo & Guélin 1987), as well as SiO and SiS belong to the first category, and the carbon chains, SiC, SiC_2 and MgNC to the second. Only CO and, to a lesser degree, HCN, are distributed throughout the envelope.

Though highly variable in the hot and dense inner envelope, the gas temperature and the gas density seem fairly constant in the $15''$ radius hollow shell: $T_k \simeq 50$ K and $n_{\rm H_2} \sim 10^4$ cm^{-3}. Most species confined in this shell have thus a rather well defined rotational temperature and their radial column densities can be calculated with some accuracy. Our calculations, based on the present $\lambda 2$ mm data, as well as on our $\lambda 3$ mm and 1.3 mm data and the data of Kawaguchi et al. (1995), assume that the rotational levels within each vibrational state follow a Boltzman distribution with a rotational temperature $T_{\rm rot}$, and that the lines are optically thin (see Guélin et al. 1997). Table 10 lists the rotation temperatures, radial column densities, and fractional abundances relative to H_2 for the species confined in the outer shell (and for which we observed enough lines to sample the partition function). For these calculations, the poorly known distance to IRC+10216 was assumed to be equal to 200 pc and the mass loss rate equal to 3 10^{-5} $M_\odot$ (Truong-Bach et al. 1991). We note that the stellar mass loss rate derived from far-infrared ISO data for the same distance is twice smaller (Cernicharo et al. 1996). Although the column density ratios depend neither of the distance, nor of the mass loss rate, the fractional abundances depend on the mass loss rate. Their uncertainties could thus be crudely estimated to be a factor of 2.

4.1.1. Oxygen-bearing compounds

The paucity of oxygen compounds is perhaps the most striking characteristic of this C-rich envelope. Only 3 O-bearing molecules are actually observed, CO, SiO and HCO^+ (Lucas & Guélin 1990), the former two trapping almost all the oxygen available in the gas phase. CO and SiO are formed in the stellar atmosphere and show centrally peaked distributions. HCO^+ appears later and is only observed farther in the envelope (Lucas & Guélin 1998).

4.1.2. Carbon chains and radicals

The large abundance of highly unsaturated carbon chains and radicals, most of which are linear, is the second characteristic feature of IRC+10216. Except for TMC 1, no other source in the sky shows such a wealth of long linear chains.

Because of the fairly high temperature, the lowest bending modes of these chains are excited and can give rise to relatively strong pure rotational lines.

Such is the case for the linear C_4H radical, which has a $^2\Sigma^+$ ground state and a low lying $^2\Pi$ electronic state. Renner-Teller interaction between these two states pushes down the lowest excited bending states, $1\nu_7$ and $2\nu_7$, to energies as low as $100 - 200$ cm^{-1} (Yamamoto et al. 1987). Rotational transitions within these states are seen throughout the 2-mm window. The lines pertaining to the $1\nu_7(^2\Pi)$ and $2\nu_7(^2\Sigma)$ states are remarkably strong with respect to the ground state lines, showing that theses excited states contain a significant fraction, $\simeq 1/7$ and $1/12$ respectively, of the total C_4H column density.

4.1.3. Cyclic compounds

Discarding SiC_2, which has a T-shaped rather than cyclic structure, only three cyclic compounds were detected in our survey: c-C_3H, c-C_3H_2, and c-SiC_3, a rhombic-shaped molecule recently discovered by Apponi et al. (1999). The paucity of cyclic compounds is another characteristic feature of IRC+10216, whose IR spectrum does not show the ubiquitous unidentified infrared bands (Cernicharo et al. 1999, in preparation). The column density of c-C_3H is only a factor of $\simeq 2$ lower than that of its linear isomer. In comparison, the abundance ratio of l-C_3H_2 over c-C_3H_2 is much smaller: ≤ 0.05 (Cernicharo et al. 1991c).

4.1.4. Silicon and metal-bearing species

The wealth of refractory Si-bearing and metal-bearing compounds is yet another characteristic of IRC+10216. The former includes SiO, SiS, SiC, SiC_2, SiC_3 and SiC_4. SiC_4, which is linear (Ohishi et al. 1989), is too heavy

to be observable at $\lambda 2$ mm. Although they are refractory, SiC and SiC_2 are mostly observed in the outer shell, whereas SiO and SiS are centrally peaked (Lucas et al. 1994). SiC was first discovered in the course of this survey (Cernicharo et al. 1989).

The diatomic metal compounds NaCl, KCl, AlCl, and AlF were also detected and identified in the course of this survey (Cernicharo & Guélin 1987). They were the first metallic molecules ever observed outside planetary or stellar atmospheres. Such a wealth of metal-bearing ionic molecules was unexpected, as most abundant species in circumstellar envelopes have covalent bonds. It opens interesting prospects on circumstellar chemistry and has stimulated laboratory work on metallic radicals.

Two magnesium-bearing radicals are detected in IRC+10216: MgNC (Guélin et al. 1986; Kawaguchi et al. 1993) and MgCN (Ziurys et al. 1995). Searches for MgCCH (Ziurys et al. in preparation), MgF and MgCl have yielded so far only upper limits.

The MgNC radical is observed in the same cold thin shell as the carbon-chain molecules and radicals, while the metal halides are concentrated in a hot region close to the star (Guélin et al. 1993). Their line intensities peak at or below 2-mm wavelength except for AlF, the lightest of these species. The $J = 15 - 14$ line of AlF, observed at 494.2 GHz with the CSO telescope at the same angular resolution as the lines of this survey, has an intensity of 12 K km s^{-1} and is 3 times stronger than the $J = 5 - 4$ transition.

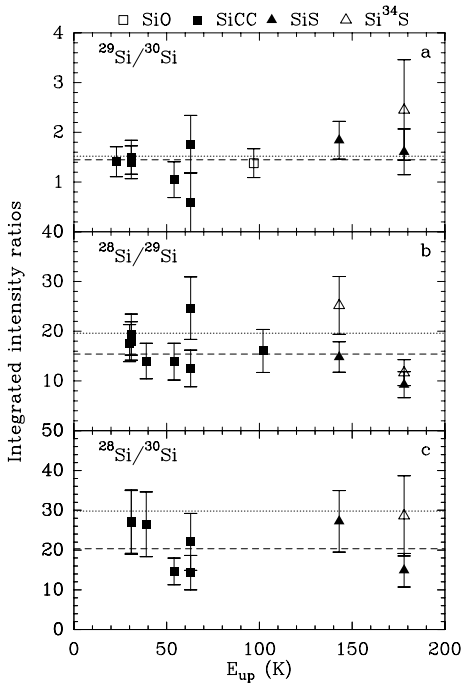

Fig. 3. The silicon isotopic abundance ratios in IRC+10216, derived from the SiS and SiC_2 line intensities. Each triangle stands for a rotational transition. The ordinate is the intensity ratio observed for two different isotopomers, after a correction in ν^{-2} had been applied (see Kahane et al. 1988). Abscissa denotes the energy (E/k) of the transition upper level

4.1.5. Phosphorus compounds

The CP radical (Guélin et al. 1990) and PN (see Fig. 2) are the only P-bearing molecules observed in this source. Whereas CP is detected only in IRC+10216, PN is seen in several warm molecular clouds (Turner et al. 1990). Besides the half-blended 140966 MHz line visible in Fig. 2, which coincides with the $J = 3 - 2$ transition of PN (see Table 2), we have observed two weak lines at 93979 MHz and near 234935 MHz, which would correspond to the $J = 2 - 1$ and $5 - 4$ transitions. The detection of PN in IRC+10216 is thus highly probable. Surprisingly, we failed to detect the stable HCP molecule, whose electron outer shell is analog to HCN (Turner et al. 1990).

4.2. Isotopic species

As shown first by Wannier (1980) and later by Kahane et al. (1988, 1992), the elemental isotopic composition of IRC+10216 is markedly non-solar, despite its location in the solar neighbourhood. Most likely, the central star CWLeo has already reached the end of the AGB phase and expelled the bulk of its convective shell. What remains of the shell is highly enriched in processed material upheaved after the ultimate dredge-ups. The very low abundance of ^{15}N, an element destroyed in equilibrium by the main CNO cycle, confirms that the gas in the outer circumstellar envelope is essentially formed of processed material. An analysis of the observed isotopic abundances of N, O and Mg in the light of stellar evolution calculations shows that CWLeo had a mass between 3 and 4 $M_\odot$ when it was on the main sequence (Guélin et al. 1995; Forestini et al. 1997).

As in our previous studies of the isotopic abundance ratios in IRC+10216 (Kahane et al. 1988, 1992; Cernicharo et al. 1986c; Cernicharo & Guélin 1987; Cernicharo et al. 1991a; Forestine et al. 1997), we have made no attempt to model the line intensities: the isotopic ratios are simply the ratios of the integrated line intensities given in Table 2, corrected for a frequency factor of ν^{-2}. For a discussion of the different biases that may affect the derivation of elemental isotopic ratios from molecular lines observations, see Kahane et al. (1988, 1992).

Except for the magnesium-bearing species, the isotopic ratios analyzed here rely on larger sets of data than previously reported so that *(i)* the biases due to line opacities can be avoided or at least easily identified, *(ii)* the error bars on the average isotopic ratios are significantly reduced. In addition, using the C_4H doublets as secondary calibrators, we were able to check the intensities of a number of spectra and eventually to correct them with a

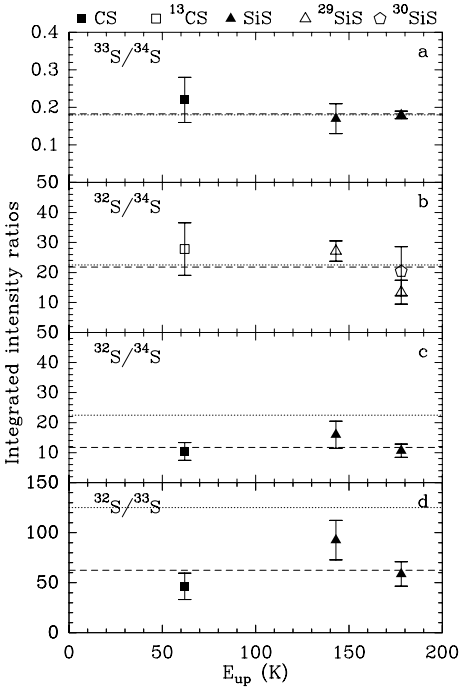

Fig. 4. Same as Fig. 3 for sulfur

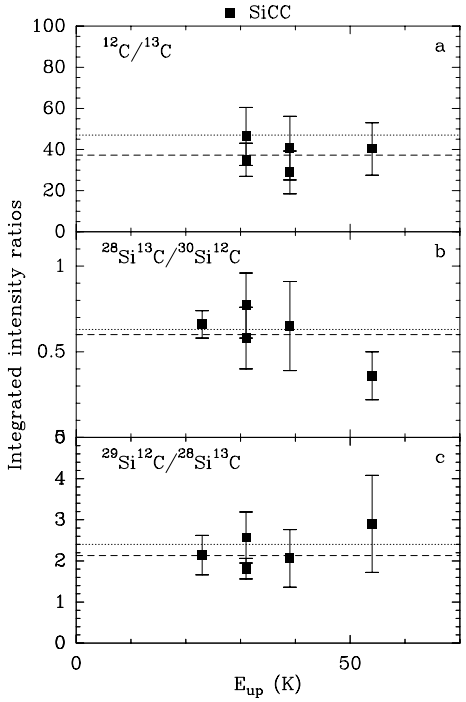

Fig. 5. Same as Fig. 3 for carbon

Table 10. Molecular column densities

Molecule	$T_{\rm rot}$ kelvin	Col. Dens.[t] cm^{-2}	Frac. abund. $N(X)/N(H_2)$
C_2H	20	5.0 10^{15}	7.1 10^{-6}
l-C_3H	20	7.0 10^{13}	1.0 10^{-8}
C_4H	35	3.0 10^{15}	4.3 10^{-6}
C_5H	25	4.4 10^{13}	6.3 10^{-8}
C_6H	35	5.5 10^{13}	7.8 10^{-8}
C_7H	35	2.2 10^{12}	3.1 10^{-9}
C_8H	52	1.0 10^{13}	1.4 10^{-8}
C_3N	20	2.5 10^{14}	3.5 10^{-7}
C_5N	35[a]	6.3 10^{12}	9.0 10^{-9}

[a] Assumed.
[t] Total column density across the source, i.e. *twice* the radial column density.

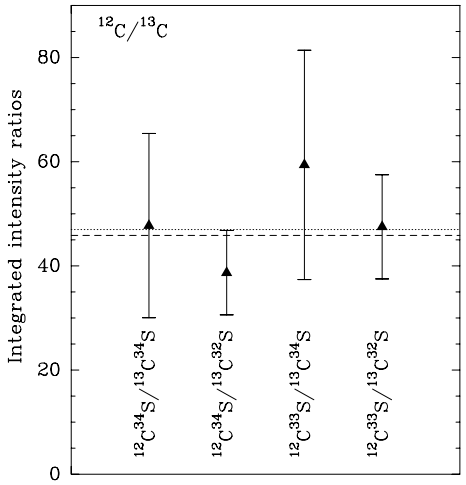

Fig. 6. The $^{12}C/^{13}C$ isotopic abundance ratios, derived from four CS transitions involving doubly substituted isotopomers. The ordinate is the intensity ratio divided by the square of the frequency ratio

reliability better than 10% rms. The results are reported in Table 11 and Figs. 3–6, together with the solar sytem values. For each intensity ratio, the rms errorbar includes two statistically independant uncertainties: a 20% calibration uncertainty (reduced to 10% when the spectrum calibration could be checked with a C_4H line) and a "fit uncertainty" (derived from a model line fit as explained in Sect. 2.2). The average isotopic ratios derived from several transitions are computed using weights inversely proportional to the individual error bars.

4.2.1. Chlorine

^{37}Cl, which is 3.1 times less abundant than ^{35}Cl in the solar system, is detected in three species: $Na^{37}Cl$, $Al^{37}Cl$

Table 11. Elemental isotopic abundance ratios

Isotopic ratio	average value	solar value	comments
$^{29}Si/^{30}Si$	1.45 (0.13)	1.52	
$^{28}Si/^{29}Si$	15.4 (1.1)	19.6	opacity
$^{28}Si/^{30}Si$	20.3 (2.0)	29.8	opacity
$^{33}S/^{34}S$	0.18 (0.1)	0.18	
$^{32}S/^{34}S$	21.8 (2.6)	22.5	
$^{32}S/^{33}S$	62 (8)	125	opacity
$^{12}C/^{13}C$	45 (3)	89	

and $K^{37}Cl$. In our detection paper (Cernicharo & Guélin 1987) we reported a $^{35}Cl/^{37}Cl$ abundance ratio of 2.4 ± 1 for aluminium chlorine and of 2 ± 1 for sodium chlorine. From the data in Tables 2 and 6 we derive for NaCl, KCl and AlCl (two lines) an average $^{35}Cl/^{37}Cl$ ratio of 3.1 ± 0.6 which is fully consistent with the solar system ratio.

4.2.2. Magnesium and aluminium

MgNC is abundant enough that the 2-mm and 3-mm lines of the rare isotopomers ^{25}MgNC and ^{26}MgNC could be detected.

The ^{24}MgNC:^{25}MgNC:^{26}MgNC abundance ratios are found equal to 78: 11 ± 1: 11 ± 1 and are consistent with the solar system ^{24}Mg:^{25}Mg:^{26}Mg isotopic ratios (79.0:10.0:11.0) (Guélin et al. 1995).

A line with a rest frequency of 234433 MHz has been tentatively identified by Guélin et al. (1995) as the $J = 7 - 6$ transition of ^{26}AlF. ^{26}Al is an element with a lifetime $t_{1/2} = 7\,10^5$ yr which is indirectly observed in the interstellar medium. Unfortunately, the present spectral survey is not sensitive enough support or infirm this identification through the observation of the $J = 5 - 4$ and/or $J = 4 - 3$ rotational transitions.

4.2.3. Silicon

Following the first identification of $^{28}SiC_2$ (Thaddeus et al. 1984; Gottlieb et al. 1989) and that of its rare isotopomers $^{29}SiC_2$, $^{30}SiC_2$ and $Si^{13}CC$ (Cernicharo et al. 1986c, 1991a), we have identified in our survey a total of 49 lines pertaining to these species. Similarly, we detected 18 lines arising from 7 isotopomers of SiS ($^{28}Si^{32}S$, ^{29}SiS, ^{30}SiS, $Si^{34}S$, $Si^{33}S$, and the doubly-substituted species $^{29}Si^{34}S$ and $^{30}Si^{34}S$). We have thus significantly enlarged our database to derive silicon isotopic ratios.

Two of the silicon isotopes, ^{29}Si and ^{30}Si, have significantly smaller abundances than the main isotope, ^{28}Si (by factors about 20 and 30 respectively in the solar system), which causes the millimeter lines of the rare SiC_2 and SiS isotopomers to be optically thin (see Cernicharo et al. 1986c, and Kahane et al. 1988, 1992). It is thus straightforward to derive the $^{29}Si/^{30}Si$ abundance ratio. All the abundance ratios derived from the integrated intensities of Tables 4 and 5 are plotted in Fig. 3a. Except for two abundance ratios which have large error bars, due to poor signal–to–noise ratio, the measurements show a small dispersion. This strenghthens the idea that the molecular lines intensity ratios faithfully reflect the silicon isotopic ratios. From 5 lines of SiCC, 2 lines of SiS and 1 line of SiO, we obtain an average $^{29}Si/^{30}Si$ abundance ratio of 1.45 ± 0.13, in good agreement with the solar system ratio of 1.52.

Derivation of the $^{28}Si/^{29}Si$ and $^{28}Si/^{30}Si$ isotopic ratios are more difficult since most of the ^{28}Si-bearing molecular lines are somewhat optically thick, leading to an underestimate of the true isotopic ratio. A way to avoid this effect is to use doubly-substituted intensity ratios, such as $^{28}Si^{34}S/^{29}Si^{34}S$. However, the rarer isotopic lines become so weak that the ratio is affected by poor signal–to–noise ratios and the risk of confusion with weak unrelated lines increases significantly. All the $^{28}Si/^{29}Si$ and $^{28}Si/^{30}Si$ abundances ratios derived from the integrated intensities of Table 4 are plotted in Figs. 3b and 3c. The average ratios are $^{28}Si/^{29}Si = 15.4 \pm 1.1$ and $^{28}Si/^{30}Si = 20.3 \pm 2.0$, i.e. respectively 1.3 and 1.5 times smaller than the solar system value. Such discrepancies are easily explained by opacity of the main isotopic lines, computed to be between 0.5 to 0.9. The analysis of the sulfur isotopomers of SiS confirm that the ^{28}SiS rotational lines, like the $C^{32}S$ ones (see below), are indeed optically thick.

We thus conclude that all the silicon isotopic ratios in the circumstellar envelope of IRC+10216 are very probably close to the solar system values.

4.2.4. Sulfur

A similar study of the sulfur isotopic ratios can be made with our data. From one line of CS and two lines of SiS, we derive for the rare sulfur isotopes an isotopic ratio $^{33}S/^{34}S = 0.18 \pm 0.01$, identical to the solar system value (see Fig. 4a).

The $^{32}S/^{34}S$ isotopic ratio can be determined from the optically thin lines of the rare isotopomers ^{13}CS, ^{29}SiS and ^{30}SiS (Fig. 4b). They provide an average value of 21.8 ± 2.6. This value appears significantly larger than the average value of 11.7 ± 1.7 derived from the optically thick lines of CS and SiS (see Fig. 4c) and quite consistent with the solar system value of 22.5. If, as is very likely, the discrepancy between both averages is due to optical depth effects on the strong CS and SiS lines, a mean opacity of about 1.4 is implied.

The $^{32}S/^{33}S$ isotopic ratio cannot be derived from doubly-substituted lines which are below our detection level. Using the single substituted species $^{28}Si^{32}S$ and $^{28}Si^{33}S$, we find an average value $^{32}S/^{33}S \simeq 62 \pm 8$ (see Fig. 3d), a factor of 2 smaller than the solar value of 125. This is just what is expected if the lines of the main isotope have opacities of the order of 1.6 (in good agreement with the estimate derived from the $^{32}S/^{34}S$ ratio).

As for the silicon, we conclude that all the sulfur isotopic ratios in the circumstellar envelope of IRC+10216 are compatible with the solar system values.

4.2.5. Carbon

We have detected 14 different ^{13}C-bearing molecular species in our 2-mm survey, including the four ^{13}C isotopomers of C_4H and the three isotopomers of C_3N. The averaged $^{12}C/^{13}C$ isotopic ratio is 45 ± 12 for C_4H and 35 ± 15 for C_3N. These ratios are mainly affected by the low line intensities of the ^{13}C species. As will be discussed in detail in a forthcoming paper (Kahane et al. 1999, in preparation) the linear carbon chains HC_3N and to a lesser extent C_4H and C_3N could show, in addition to a moderate opacity of the main isotopomer lines, isotopic fractionation so that they cannot be easily used to derive the elemental $^{12}C/^{13}C$ isotopic ratio. We will thus focus here on the SiCC and CS lines.

The six transitions observed both for SiCC and for its ^{13}C-bearing isotope in our 2-mm survey yield an average isotopic ratio of 37 ± 5 (see Fig. 4a), significantly smaller than the solar value of 89, but somewhat smaller than the value of 47 derived by Kahane et al. (1988) from optically thin lines. If attributed to the opacity of the main lines, this discrepancy leads to an optical depth of 0.5, in very good agreement with the estimates derived from the silicon isotopomer analysis.

The silicon isotopic ratios being very probably close to solar, we may also use the optically thin doubly-substituted species to derive the $^{12}C/^{13}C$ ratio. In Fig. 4b, we have plotted the five intensity ratios derived from Si^{13}CC and ^{30}SiCC. They correspond to an average value of 0.60 ± 0.06 for the double isotopic ratio ($^{13}C/^{12}C$)($^{28}Si/^{20}Si$). Assuming a solar ($^{28}Si/^{30}Si$) ratio, it leads to a $^{12}C/^{13}C$ isotopic ratio of 50 ± 7, in good agreement with our previous estimate. Similarly, the observations of ^{29}SiCC allow us to derive an average ($^{12}C/^{13}C$)($^{29}Si/^{28}Si$) ratio of 2.1 ± 0.2. With a solar ($^{28}Si/^{29}Si$) ratio, it corresponds to a $^{12}C/^{13}C$ isotopic ratio of 41 ± 4, also in agreement with the previous values.

With the four rare isotopes of CS (see Table 9) we may also derive $^{12}C/^{13}C$ ratios free of opacity effects. These ratios are obtained directly from $^{12}C^{34}S/^{13}C^{34}S$, and using solar values for the sulfur isotopic ratios for the other pairs of lines. They have a small dispersion (see Fig. 5) and one calculates an average value of 46 ± 6, also very close to the previous estimates.

In conclusion, when averaging the three $^{12}C/^{13}C$ ratios derived from optically thin lines of SiCC and CS, we obtain a value of 45 ± 3, in very good agreement with the value given in Kahane et al. (1988) and Cernicharo et al. (1991a).

A sensitive search for ^{14}CO (Forestini et al. 1997), carried out at 1.3 and 2.6 mm, yielded only low upper limits to the abundance of this species and to the ^{14}C:^{12}C isotopic abundance ratio ($< 2\,10^{-5}$), despite an earlier claim by Wright (1994) for its detection.

4.3. Unidentified lines

The list of U-lines is given in Table 3. Some of these lines could be arising from vibrationally excited states of well known molecules, just as we see many lines pertaining to the $\nu_7 = 1$ state of HC_3N (see Table 8), the $\nu_7 = 1$, 2 states of C_4H (see Table 7), the $v = 1$, 2, 3 states of SiS (see Table 4), the $v = 1$ of CS (see Table 9), and the $\nu_3 = 1$ state of SiC_2 (see Table 5). Potential candidates could be the low-lying bending states of C_5H, C_6H, MgNC and NaCN whose spectroscopic constants are poorly known. However, taking into account the intensity of the ground state lines of these species, the vibrationally excited states could only account for the weak U lines.

The stronger U-lines must arise from new, not yet identified, molecular species. No harmonic relation exists between any subset of them. They could arise either from asymmetric top molecular species, or from species with non-zero electronic angular momentum. Surprisingly, only few asymmetric top molecules have been so far identified in IRC+10216. This probably results from the small number of asymmetric top radicals studied in the laboratory and from the difficulty to identify ab initio such species in IRC+10216's spectrum. We are currently searching for characteristic spectroscopic patterns at 3 mm and 1 mm in order to allow the identification of the carriers.

4.4. Other molecular species

Many other molecules and radicals of astrophysical interest, such as MgH, MgO, CCN, CCO, KCN, H_2CS, CH_3OH, H_2CO, HNCO, Si_2H_2, H_2CSi, H_2C_2Si, have strong lines within the frequency range covered by our survey, but have not been detected. It is difficult, however, to set significant upper limits to their abundances, as long as their spatial distributions and rotation temperatures remain unknown.

4.5. Vibrationally excited species

Many lines of the mm-wave spectrum of IRC+10216 correspond to rotational transitions inside vibrationally excited states. As we have seen (see also Guélin et al. 1987b; Yamamoto et al. 1987), the $1\nu_7(^2\Pi)$, $2\nu_7(^2\Sigma)$, and $2\nu_7(^2\Delta)$ bending states of the ground $^2\Sigma^+$ electronic state of C_4H give rise to an impressive number of lines in the 2-mm and 3-mm bands. Other such lines arise from C_3H (Guélin et al. 1998), HCN, HC_3N, CS (Turner 1987a), SiS (Guélin et al. 1987b; Turner 1987b), SiC_2 (Forestini et al. 1997) and MgNC (Guélin et al. 1997). It is worth noting that despite sensitive searches, no vibrationally excited lines have been detected so far for C_2H, C_3N (Murakami et al. 1989),

SiC (Mollaaghababa et al. 1990). There is a weak feature (0.03 K) at the frequency of the $v = 1$ $J = 2 - 1$ line of CO; unfortunately the $J = 1 - 0$ line is blended with C_4H. Observations of higher J lines are needed to confirm the detection of vibrationally excited carbon monoxide in IRC+10216.

5. Conclusions

We have carried out a frequency sweep of the carbon-rich star IRC+10216 between 129 and 172.5 GHz. 380 lines were detected, of which 317 have been identified and assigned to 30 different molecular species.

The most recurrent molecule in IRC+10216's 2 mm spectrum is C_4H, whose different isotopomers and vibrationally excited states give rise to 60 lines. It is followed by SiC_2, with 44 lines from the three stable silicon isotopomers and from $Si^{13}CC$. NaCN with 23 lines is also a major polluant of the spectrum.

HC_3N and its isotopomers account for 21 lines. Other carbon chains like HCCN, C_3H, CH_3CN, HC_5N, C_3N, H_2C_4 (Cernicharo et al. 1991b), C_5H and C_6H account for 75 lines. Altogether, the above carbon chain molecules give rise to 36% of lines observed in the 2-mm window, a proportion which rises to 41% if the C_nS chains are included.

The main characteristics of the IRC+10216 molecular envelope, compared to warm and dense interstellar clouds with similar physical conditions, are *i)* the large number of carbon chain molecules and radicals, as well as of silicon, sulfur and metallic compounds, and *ii)* the small number of saturated species and oxygen compounds. As a result, the 2-mm spectra of IRC+10216 and Orion A (see Ziurys & McGonagle 1993) look almost orthogonal, i.e. show a remarkably small number of common lines.

Acknowledgements. The present survey includes spectra taken in collaboration with J. Gómez-González, S. Saito, S. Yamamoto and L. Ziurys, who we would like to thank. This work has been partially supported by the Spanish DGICYT under grants PB90-408, PB93-048, PB96-0883 and PNIE98-1351E. J. Cernicharo was at CNRS–Observatoire de Grenoble when the survey was initiated and stayed at the Observatorio Astronómico Nacional (OAN) for several years while working on the data.

References

Apponi A.J., McCarthy M.C., Gottlieb C.A., Thaddeus P., 1999, ApJ 516, L103
Avery L., Amano T., Bell M.B., et al., 1992, ApJS 83, 367
Cernicharo J., 1985, ATM "A Program to compute atmospheric absorption for frequencies below 1000 GHz", IRAM Internal Report No. 52
Cernicharo J., 1988, Ph.D. Thesis, Université de Paris VII
Cernicharo J., Kahane C., Gómez-González J., Guélin M., 1986a, A&A 164, L1
Cernicharo J., Kahane C., Gómez-González J., Guélin M., 1986b, A&A 167, L5
Cernicharo J., Kahane C., Gómez-González J., Guélin M., 1986c, A&A 167, L9
Cernicharo J., Guélin M., Walmsley C.M., 1987a, A&A 172, L5
Cernicharo J., Guélin M., Menten K.M., Walmsley C.M., 1987b, A&A 181, L1
Cernicharo J., Guélin M., Hein H., Kahane C., 1987c, A&A 181, L9
Cernicharo J., Guélin M., 1987, A&A 183, L10
Cernicharo J., Gottlieb C.A., Guélin M., Thaddeus P., Vrtilek J.M., 1989, ApJ 341, L25
Cernicharo J., Guélin M., Kahane C., Bogey M., Demuynck C., Destombes J.L., 1991a, A&A 246, 213
Cernicharo J., Gotlieb C.A., Guélin M., Killian T.C., Thaddeus P., Vrtilek J.M., 1991, ApJ 368, L43
Cernicharo J., Gotlieb C.A., Guélin M., et al., 1991, ApJ 368, L41
Cernicharo J., Barlow M., González-Alfonso E., et al., 1996, A&A 315, L201
Cernicharo J., Guélin M., 1996, A&A 309, L27
Demaison J., et al., 1974, Landolt-Börnstein: Atomic and Molecular Physics Vol. 6: Molecular Constants, Hellwege & Hellwege (eds.). Springer-Verlag, Berlin
Forestini M., Guélin M., Cernicharo J., 1997, A&A 317, 883
Gottlieb C.A., Gottlieb E.W., Thaddeus P., 1986, A&A 164, L5
Gottlieb C.A., Vrtilek J., Thaddeus P., 1989, ApJ 343, L29
Glassgold A.E., 1996, ARA&A 34, 241
Gordy W., Cook R.L., 1984, Microwave Molecular Spectra, Techniques of Chemistry Vol. XVIII. John Wiley & Sons, New York, p. 81
Groesbeck T.D., Phillips T.G., Blake, Geoffrey A., 1994, ApJ 428, 680
Guélin M., Cernicharo J., Kahane C., Gómez-González J., 1986, A&A 157, L17
Guélin M., Cernicharo J., Kahane C., Gómez-González J., Walmsley C.M., 1987a, A&A 175, L5
Guélin M., Cernicharo J., Navarro S., Woodward C.R., Gotlieb C.A., Thaddeus P., 1987b, A&A 182, L37
Guélin M., Cernicharo J., Paubert G., Turner B., 1990, A&A 230, L9
Guélin M., Cernicharo J., 1991, A&A 244, L21
Guélin M., Lucas R., Cernicharo J., 1993, A&A 280, L19
Guélin M., Forestini M., Valiron P., et al., 1995, A&A 297, 183
Guélin M., Lucas R., Neri R., 1997, in: CO: Twenty-Five Years of Millimeter-Wave Spectroscopy, Proc. IAU Symp. 170, Latter W.B. et al. (eds.). Kluwer, Dordrecht, p. 359
Guélin M., Cernicharo J., Travers M.J., et al., 1997, A&A 317, 883
Guélin M., Cernicharo J., Travers M.J., et al., 1998, A&A 317, 883
Johansson L.E.B., Anderson C., Elder J., et al., 1985, A&AS 60, 135
Kahane C., Gómez-González J., Cernicharo J., Guélin M., 1988, A&A 190, 167
Kahane C., Cernicharo J., Gómez-González J., Guélin M., 1992, A&A 256, 235

Kawaguchi K., Kagi E., Hirano T., Takano S., Saito S., 1993, ApJ 406, L39
Kawaguchi K., Kasai Y., Ishikawa S., Kaifu N., 1995, PASJ 47, 853
Lovas F.J., 1978, J. Phys. Chem. Ref. Data 7, 1445
Lovas F.J., 1986, J. Phys. Chem. Ref. Data 15, 251
Lovas F.J., Tiemann 1974, J. Phys. Chem. Ref. Data 3, 611
Lucas R., Guélin M., 1990, in "Submillimetre Astronomy". Kluwer Academic Publishers, The Netherlands , p. 97
Lucas R., Guélin M., 1998, in: IAU Symp. 191, Montpellier, France
Lucas R., Guélin M., Kahane C., Audinos P., Cernicharo J., 1994, Astrophys. Sp. Sci. 224, 293
Lucas R., Cernicharo J., 1989, A&A 218, L20
Murakami H., Yamamoto S., Saito S., Guélin M., 1989, A&A 217, L5
Mollaaghababa R., Gottlieb C.A., Vrtilek J.M., Thaddeus P., 1990, ApJ 352, L21
Morris M., 1985, in: Mass Loss from Red Giants, Morris M. & Zuckerman B. (eds.). Pub. Reidel, Dordrecht
Ohishi M., Kaifu N., Kawaguchi K., et al., 1989, A&A 345, L830
Poynter R.L., Pickett H.M., 1984, Submillimeter, Millimeter and Microwave Spectral Line Catalogue, JPL Publi. 80-23
Thaddeus P., Cummins S.E., Linke R.A., 1984, ApJ 283, L45
Truong-Bach, Morris D., Nguyen-Rieu, 1991, A&A 249, 435
Turner B.E., 1987, A&A 182, L15
Turner B.E., 1987, A&A 183, L23
Turner B.E., Tsuji T., Bally J., Guélin M., Cernicharo J., 1990, ApJ 365, 569
Vogt J., 1998, Microwave Catalogue, Universität Ulm Sektion für Spektren- und Strukturdokumentation, Ulm
Wannier P., 1980, ARA&A 18, 399
Wright G.A., 1994, ApJ 436, L157
Yamamoto S., Saito S., Guélin M., Cernicharo J., Suzuki H., Ohishi M., 1987, ApJ 323, L149
Ziurys L.M., McGonagle D., 1993, ApJSS 89, 155
Ziurys L.M., Guélin M., Cernicharo J., 1995, ApJ 445, L47